

Chapter 6

Underwater granular flows

6.1 Introduction

Avalanches, landslides, and debris flows are geophysical hazards, which involve rapid mass movement of granular solids, water, and air as a single phase system. Globally, landslides cause billions of pounds in damage, and thousands of deaths and injuries each year. Hence, it is important to understand the triggering mechanism and the flow evolution. The momentum transfer between the discrete and continuous phases significantly affects the dynamics of the flow as a whole (Topin et al., 2012). Although certain macroscopic models are able to capture simple mechanical behaviours (Peker and Helvacı, 2007), the complex physical mechanisms occurring at the grain scale, such as hydrodynamic instabilities, formation of clusters, collapse, and transport, (Topin et al., 2011) have largely been ignored. In particular, when the solid phase reaches a high volume fraction, the strong heterogeneity arising from the contact forces between the grains, and the hydrodynamic forces, are difficult to integrate into the homogenization process involving global averages.

In order to describe the mechanism of immersed granular flows, it is important to consider both the dynamics of the solid phase and the role of the ambient fluid (Denlinger and Iverson, 2001). The dynamics of the solid phase alone is insufficient to describe the mechanism of granular flow in a fluid. It is important to consider the effect of hydrodynamic forces that reduce the weight of the solids inducing a transition from dense-compacted to dense-suspended flows, and the drag interactions which counteract the movement of the solids (Meruane et al., 2010). Transient regimes characterized by change in the solid fraction, dilation at the onset of flow and development of excess pore pressure, result in altering the balance between the stress carried by the fluid and that carried by the grains, thereby changing the overall behaviour of the flow.

The presence of a fluid phase in a granular medium has profound effects on its mechanical behaviour. In dry granular media the rheology is governed by grain inertia and static stresses sustained by the contact network depending on the shear-rate and confining pressure, respectively (Midi, 2004). As the fluid inertia and viscosity come into play, complications arise as a result of contradictory effects. On one hand, the fluid may delay the onset of granular flow or prevent the dispersion of the grains by developing negative pore pressures (Pailha et al., 2008; Topin et al., 2011). On the other hand, the fluid lubricates the contacts between grains, enhancing in this way the granular flow, and it has a retarding effect at the same time by inducing drag forces on the grains. The objective of the present study is to understand the differences in the mechanism of flow initiation and kinematics between dry and submerged granular flow. In the present study, 2D Lattice-Boltzmann and Discrete Element Method is used to model the fluid-soil interactions in underwater granular flows.

12 6.2 Granular collapse in fluid

13 The collapse of a granular column, which mimics the collapse of a cliff, has been extensively
 14 studied in the case of dry granular material, when the interstitial fluid plays no role (see ??). The
 15 problem of the granular collapse in a liquid, which is of importance for submarine landslides,
 16 has to our knowledge attracted less attention (Rondon et al., 2011). Thompson and Hupper
 17 (2007) observed that the presence of liquid dramatically changes the way a granular column
 18 collapses compared to the dry case. The destabilization of a granular pile strongly depends on
 19 the initial volume fraction of the packing. For dense packings the granular flow is localized at
 20 the free surface of the pile, whereas for loose packings the destabilization occurs in the bulk of
 21 the material and has a parabolic profile (Bonnet et al., 2010; Iverson, 2000; Topin et al., 2011).
 22 In the present study, the collapse of a granular column in fluid is studied using 2D LBM - DEM
 23 and the flow kinematics is compared with dry granular collapse. The role of permeability and
 24 initial volume fraction on the run-out behaviour is also investigated.

25 6.2.1 LBM-DEM Coupling

26 Lattice Boltzmann approach can accommodate large grain sizes and the interaction between the
 27 fluid and the moving grains can be modelled through a relatively simple fluid – grain interface
 28 treatment. Further, employing the Discrete Element Method (DEM) to account for the grain –
 29 grain interaction naturally leads to a combined LB – DEM procedure (Mansouri et al., 2009).

30 In this study, a 2D poly-disperse system ($d_{max}/d_{min} = 1.8$) of circular discs in fluid is used to
 31 simulate the behaviour of granular collapse in fluid (see Figure 6.1). A cumulative β distribution

6.2 Granular collapse in fluid

3

- ³² is adopted to generate grains with d_{max} and d_{min} as 1.25 mm and 2.2 mm, respectively. The soil column is modelled using ≈ 2000 discs of density 2650 kg m^{-3} and a contact friction angle of 26° . A linear-elastic contact model is used in DEM simulations. The collapse of the column was simulated inside a fluid with a density of 1000 kg m^{-3} and a kinematic viscosity of $1 \times 10^{-6} \text{ m}^2 \text{ s}^{-1}$. The gravity angle θ is set to zero to simulate collapse onto a horizontal surface. The choice of a 2D geometry has the advantage of cheaper computational effort than a 3D case, making it feasible to simulate very large systems.

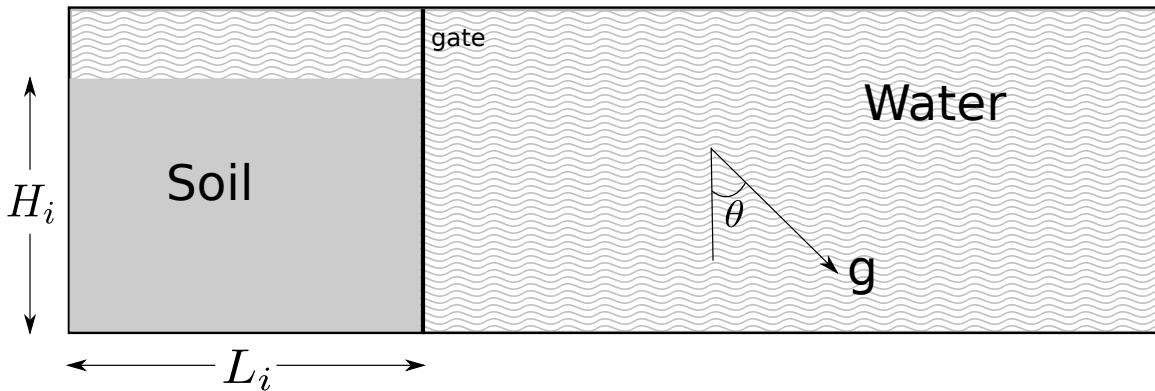


Figure 6.1 Underwater granular collapse set-up.

The Eulerian nature of the LBM formulation, together with the common explicit time step scheme of both LBM and DEM makes this coupling strategy an efficient numerical procedure for the simulation of grain – fluid systems. The critical time step for DEM is computed based on the local contact natural frequency and damping ratio. A sub-cycling time integration is adopted in DEM (see ??). A fluid flow (LBM) time step, $\Delta t = 2.0E^{-5}\text{s}$ is determined based on the viscosity and relaxation parameter $\tau = 0.506$. An integer ratio n_s , between the fluid flow time step Δt and DEM time step Δt_D is determined as 15, i.e., every LBM iteration involves a sub-cycle of 15 DEM iterations.

In order to capture realistic physical behaviour of the fluid – grain system, it is essential to model the boundary condition between the fluid and the grain as a non-slip boundary condition, i.e. the fluid near the grain should have similar velocity as the grain boundary. The solid grains inside the fluid are represented by lattice nodes. The discrete nature of lattice, results in a stepwise representation of the surfaces (see figure 6.2), which are circular, hence sufficiently small lattice spacing h is required. The smallest DEM grain in the system controls the length of the lattice spacing. In the present study, a very fine discretisation of $d_{min}/h = 10$ is adopted, i.e., the smallest grain with a diameter d_{min} in the system is discretised into 100 lattice nodes ($10h \times 10h$). This represents a very accurate representation of the interaction between the solid and the fluid nodes.

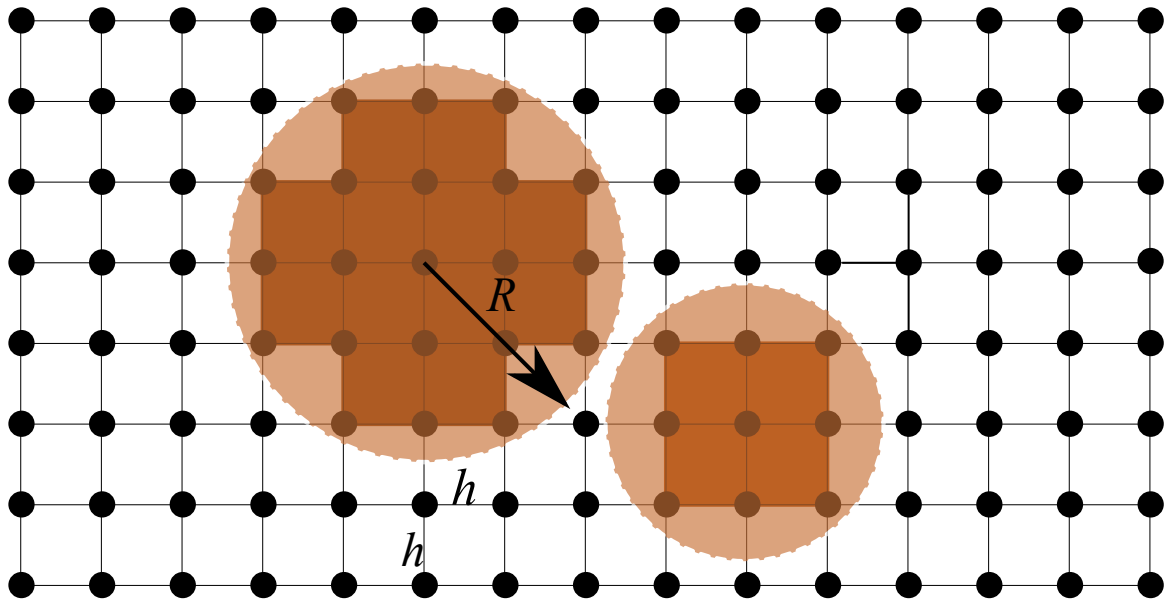


Figure 6.2 Discretisation of solid grains in LBM grid. Shows the step-wise representation of circular disks in the lattice.

¹ 6.2.2 Permeability

² In DEM, the grain – grain interaction is described based on the contact interactions. In a
³ 3D granular assembly, the pore spaces between grains are interconnected, whereas in a 2-D
⁴ assembly, the grains are in contact with each other and this results in a non-interconnected
⁵ pore-fluid space. Which means that the pore-fluid enclosed between the grains cannot flow
⁶ to neighbouring pore-space. This results in an unnatural no flow condition in a 2-D case
⁷ (see figure 6.3). In order to overcome this difficulty, a reduction in radius is assumed only
⁸ during LBM computations (fluid and fluid – solid interaction). The reduced radius of the soil
⁹ grain, i.e., the *hydrodynamic radius* ‘ r ’, allows for interconnected pore space through which
¹⁰ the pore-fluid can flow similar to 3D behaviour. The reduction in radius is assumed only
¹¹ during LBM computations, hence this technique has no effect on the grain – grain interactions
¹² computed using DEM.

¹³ Realistically, the hydrodynamic radius can be varied from $r = 0.7R$ to $0.95R$, where ‘ R ’
¹⁴ is the grain radius. Different permeability can be obtained, for any given initial packing, by
¹⁵ varying the hydrodynamic radius of the grains, without changing the actual granular packing.
¹⁶ Hence, the hydrodynamic radius represents the permeability of the granular assembly. In
¹⁷ another sense, the hydrodynamic radius can be assumed to represent the irregularities on the
¹⁸ granular surface. Reducing the hydrodynamic radius represents wider channel and more flow
¹⁹ between the grains.

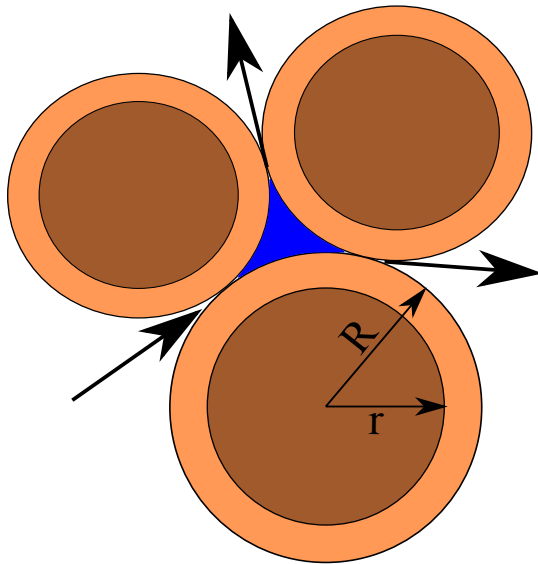


Figure 6.3 Schematic representation of the hydrodynamic radius in LBM-DEM computation

In order to understand the relation between the hydrodynamic radius and the permeability of the granular assembly, horizontal permeability tests are performed by varying the hydrodynamic radius as $0.7R$, $0.75R$, $0.8R$, $0.85R$, 0.9 and $0.95R$. A square sample of $50\text{ mm} \times 50\text{ mm}$ is used to determine the transverse permeability. Dirichlet boundary condition (discussed in ??), i.e., pressure/density constrain is applied along the left and the right boundaries. The density on the left boundary is increased in small increments ($10^{-4}\Delta P$), which a constant density is maintained on the right boundary. This results in a pressure gradient causing the fluid to flow (see figure 6.4).

The mean velocity of flow (v) is determined and the permeability of the sample (k) is computed as:

$$k = v \cdot \mu \cdot \frac{\Delta x}{\Delta P}, \quad (6.1)$$

where μ is the dynamic viscosity of the fluid (Pa s), Δx is the thickness of the bed of porous medium m , and ΔP is the applied pressure difference Pa . For a given hydrodynamic radius, the pressure gradient ΔP is varied to obtain different flow rates. Probing the fluid space showed a Poiseuille flow behaviour between grains. The flow is still within the Darcy's laminar flow regime, which is verified by the linear slope between the pressure gradient and mean flow velocity (see figure 6.5). It can be observed that with increase in the hydrodynamic radius the permeability decreases, i.e., the slope of the mean flow velocity to the pressure gradient decreases. At very low pressure gradient ($\Delta P \leq 0.1$), both $0.9R$ and $0.95r$ has a no flow condition. A hydrodynamic radius of $r = 0.95R$ shows almost no flow behaviour, even at higher pressure gradients. A high value of hydrodynamic radius $r > 0.95R$ results in unnatural flow

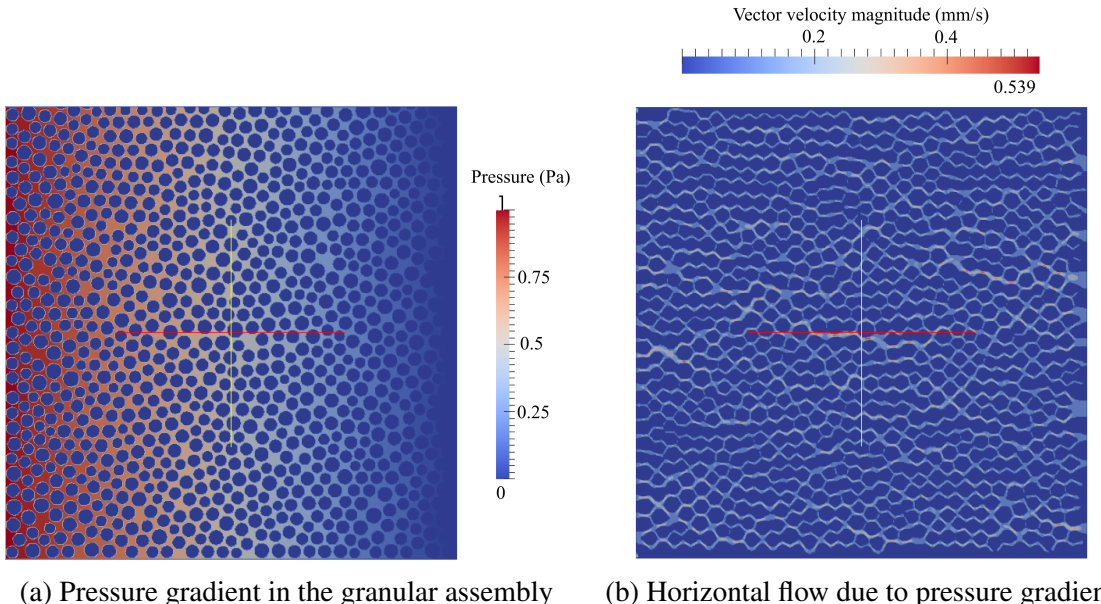


Figure 6.4 Evaluation of the horizontal permeability for a hydrodynamic radius of 0.7R.

behaviour. Hence, hydrodynamic radii in the range of 0.7 to 0.95R are adopted in the present study. 21
1

Increase in the hydrodynamic radius from 0.7 to 0.95 reduces the porosity from 0.60 to 0.27. The permeability computed from LB – DEM method is verified by comparing it with the analytical solution. One of the widely used analytical solution for permeability is the Carman – Kozeny equation (CK Model), which is based on the Poiseuille flow through a pipe and is mainly used for 3D, homogeneous, isotropic, granular porous media at moderate porosities. In the present study, a modified Carman – Kozeny equation that takes into account the micro-structure of the fibres and that is valid in a wide range of porosities is adopted ([Yazdchi et al., 2011](#)). The normalized permeability is defined as 2
3
4
5
6
7
8
9

$$\frac{k}{d^2} = \frac{\varepsilon}{\psi_{CK}(1-\varepsilon)^2}. \quad (6.2) \quad 10$$

In the CK model, the hydraulic diameter D_h , is expressed as a function of measurable quantities: porosity and specific surface area 11
12

$$D_h = \frac{4\varepsilon V}{S_v} = \frac{\varepsilon d}{(1-\varepsilon)}, \quad (6.3) \quad 13$$

$$a_v = \frac{\text{grain surface}}{\text{grain volume}} = \frac{S_v}{(1-\varepsilon V)} = \frac{4}{d}, \quad (6.4) \quad 14$$

21
1
2
3
4
5
6
7
8
9

11
12

13
14
15

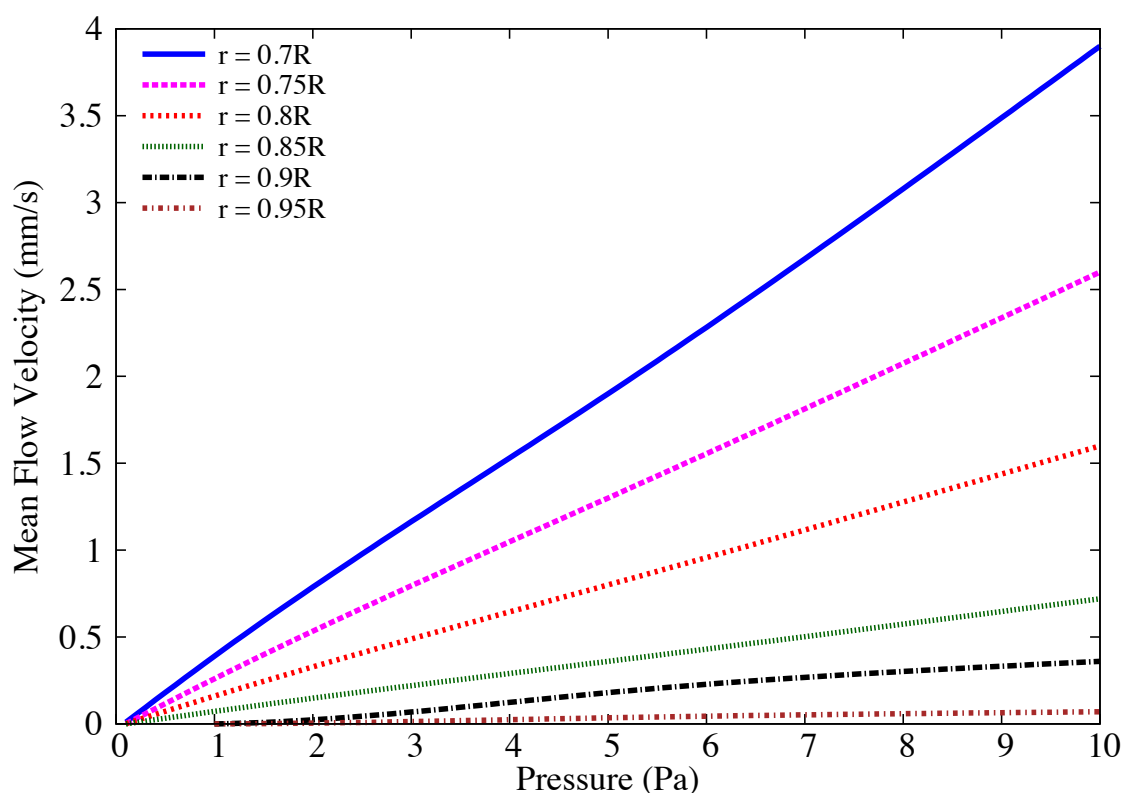


Figure 6.5 Variation of the mean flow velocity with pressure gradient for different hydrodynamic radius.

where S_v is the total wetted surface, and a_v is the specific surface area. The above value of a_v is for circles (cylinders) - for spheres $a_v = 6/d$. ψ_{CK} is the empirically measured CK factor, which represents both the shape factor and the deviation of flow direction from that in a duct. It is approximated for randomly packed beds of spherical grains. The normalized permeability for different porosity obtained by varying the radius from 0.7 to 0.95 is presented in figure 6.6. The normalized permeability is found to match the qualitative trend of the Carman-Kozeny equations. The LB – DEM permeability curve lies between the permeability curves for spherical and cylindrical grain arrangements implying a better approximation of permeability in 2D granular assembly by reducing the radius during LBM computations.

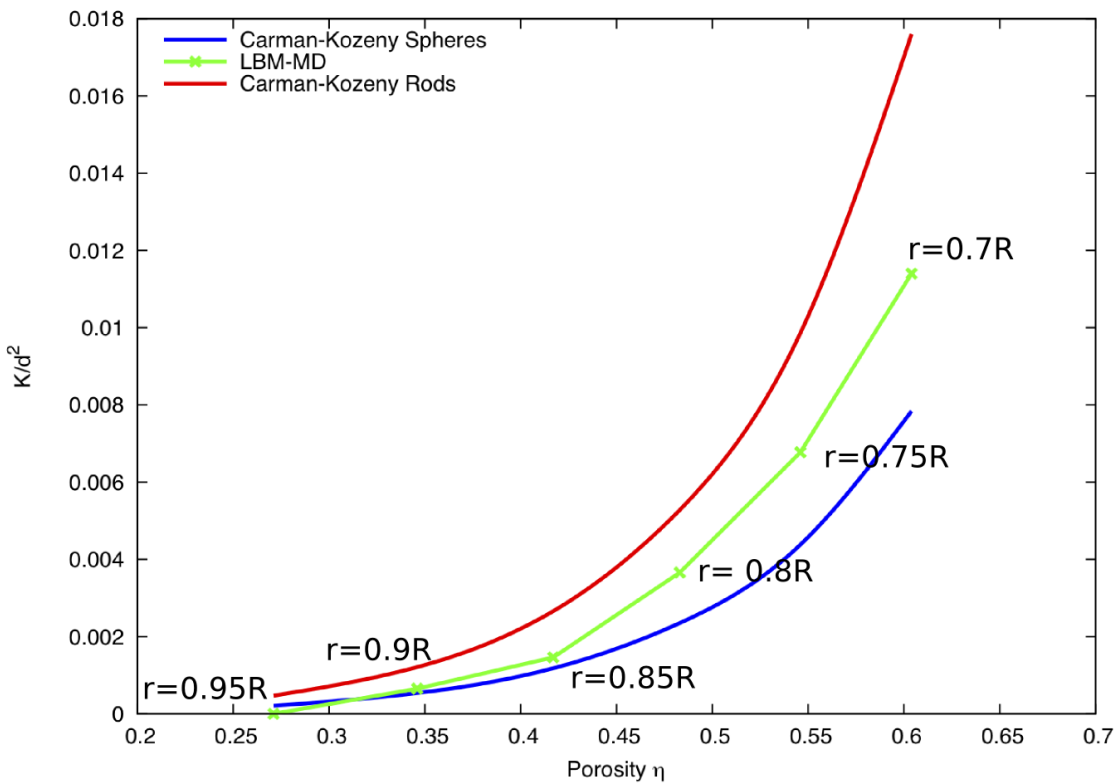


Figure 6.6 Relation between permeability and porosity for different hydrodynamic radius and comparison with the analytical solution.

6.2.3 Collapse in fluid: Flow evolution

Two-dimensional plane-strain LBM-DEM simulations of granular column collapse are performed by varying the initial aspect ratio of the column from 0.2 to 6. A hydrodynamic radius of 0.7R is adopted during LBM computations. The granular assemble has a packing fraction of 83%. The normalized final run-out distance is computed as $\Delta L = (L_f - L_0)/L_0$. Similar to

6.2 Granular collapse in fluid

9

dry granular collapse, the duration of collapse is normalised with a critical time $\tau_c = \sqrt{H/g}$. Where, H is the initial height of the granular column and g is the acceleration due to gravity. Dry and buoyant analyses of granular column collapse are also performed to understand the effect of hydrodynamic forces on the run-out distance.

Snapshots of flow evolution of a granular column collapse with an initial aspect ratio of 0.4 is shown in figure 6.7. The failure begins at the toe end of the column, and the fracture surface propagates into the column at an angle of about 50° , similar to dry column. For the short column, the failure is due to collapse of the flanks. Once the material is destabilised, the granular mass interacts with the surrounding fluid resulting in formation of turbulent vortices. These vortices interact with the grains at the surface, resulting in irregularities on the free surface. Force chains can be observed in the static region of collapse, which indicates the flow can be described using a continuum theory. As the granular material ceases to flow, force chains develop at the flow front, revealing consolidation of the granular mass resulting in increase in strength.

The evolution of run-out with time for a short column ($a = 0.4$) is presented in figure 6.8. The dry column exhibits longer run-out distance in comparison to the submerged column. The collapse of a dry column using DEM represents a collapse in vacuum, without any influence of drag forces or viscosity of air. A LBM-DEM simulation of a granular column collapse using the kinematic viscosity of air is performed to compare the dry column with the collapse in air. It can be observed that both the “dry” condition and the collapse in air show almost the same run-out behaviour. However, the collapse in fluid (water) results in a much shorter run-out distance. The granular mass in fluid has the buoyant mass, in contrast to the dry density. A dry granular collapse with the buoyant unit weight is performed to understand the effect of buoyancy on the run-out behaviour. The dry column with buoyant unit weight also exhibits longer run-out behaviour than the collapse in fluid. However, due to decrease in the initial potential energy, the run-out observed in the buoyant condition is shorter than the dry condition. The column collapse in fluid takes longer to evolve when submerged in water, which might be due to the development of large negative porewater pressure that is generated during the shear failure along the fracture surface. The large negative pore pressure has to be dissipated before the granular mass above the fracture surface can collapse and flow. The shorter run-out distance in the fluid case, in comparison with the dry and buoyant conditions, shows that the collapse in fluid is significantly affected by the hydrodynamic drag force acting on the soil grains. The evolution of height H/L is presented in ???. Since the failure of the column is only at the flank, the central static region remains unaffected. Hence, the final height of the column is the same in dry and submerged conditions.

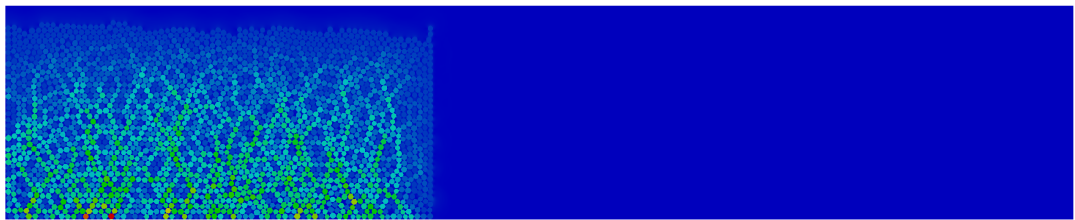
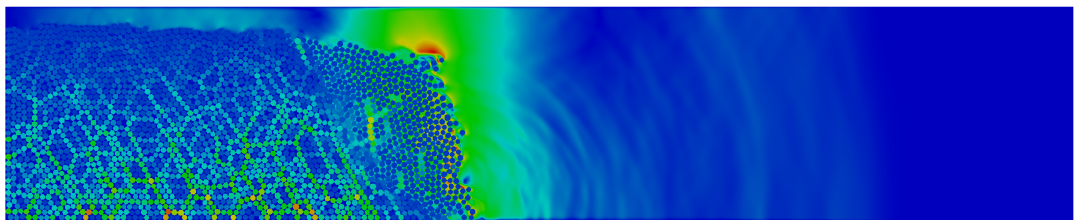
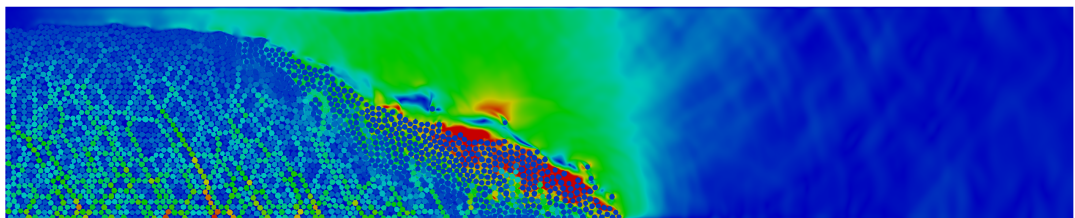
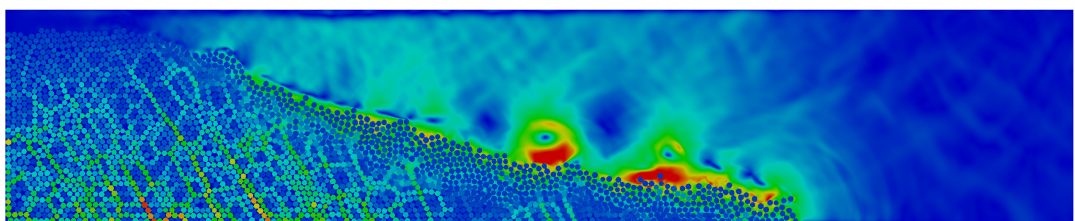
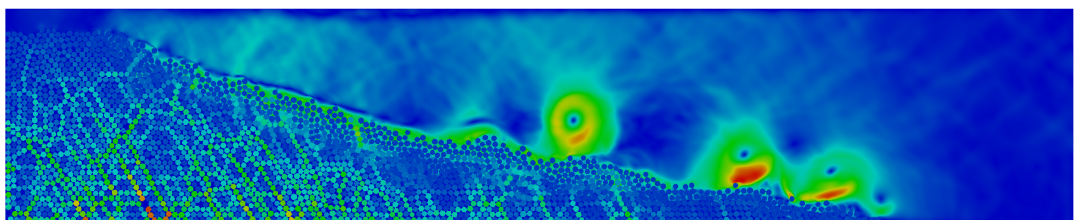
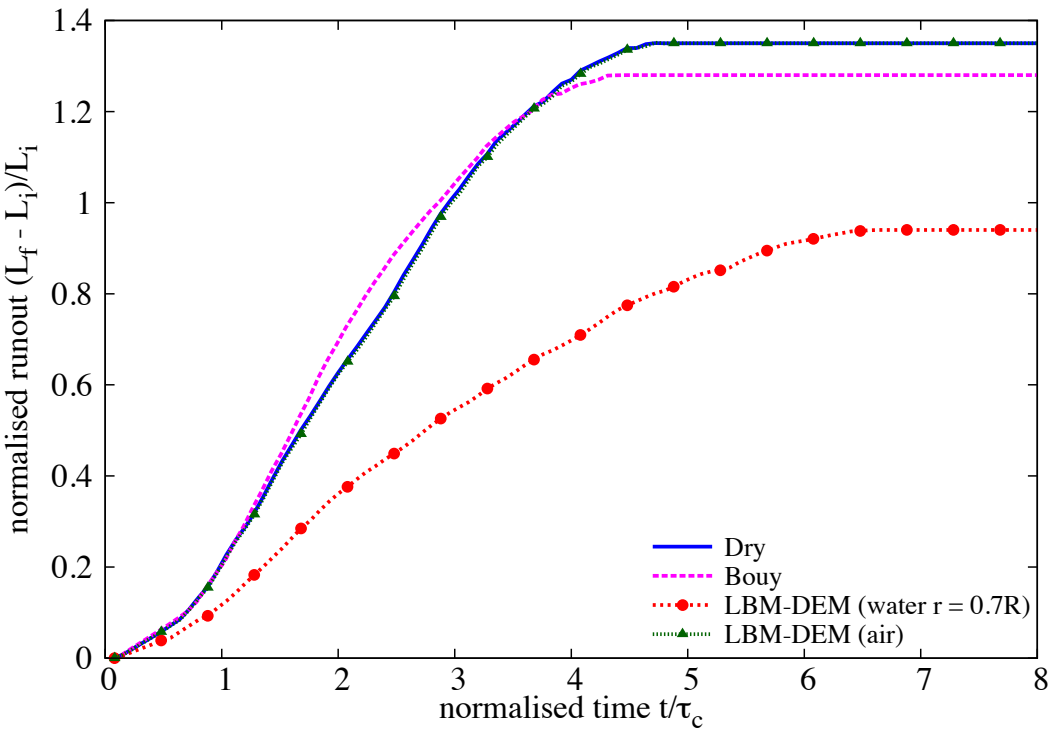
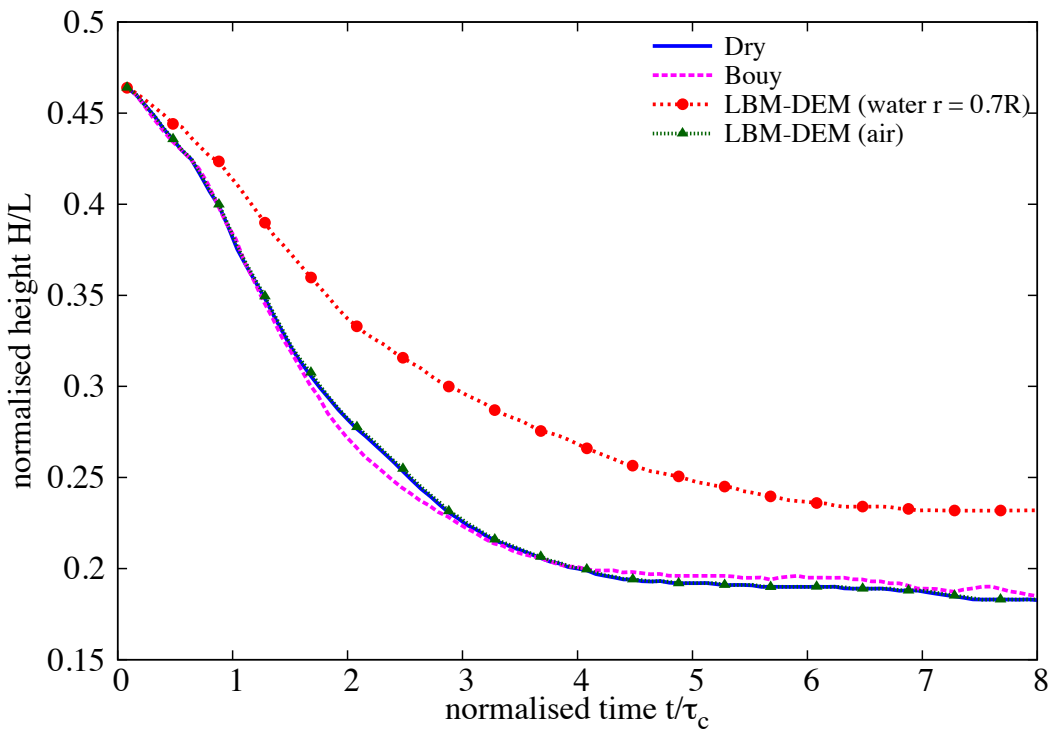
(a) $t = 0\tau_c$ (b) $t = 1\tau_c$ (c) $t = 3\tau_c$ (d) $t = 6\tau_c$ (e) $t = 8\tau_c$

Figure 6.7 Flow evolution of a granular column collapse in fluid ($a = 0.4$). Shows the velocity profile of fluid due to interaction with the grains (red - higher velocity).

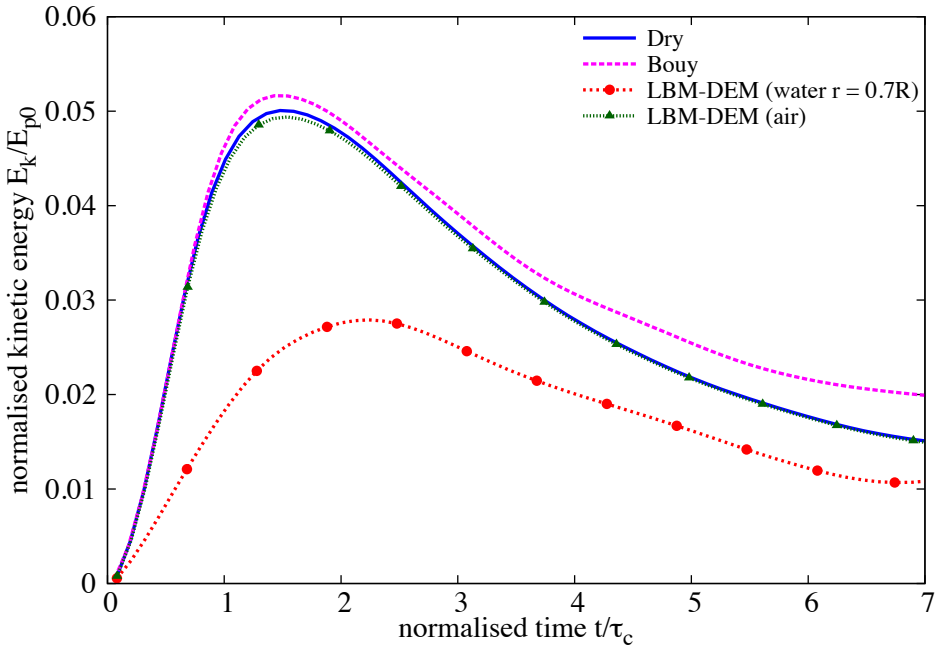
Figure 6.8 Evolution of run-out for a column collapse in fluid ($a = 0.4$)Figure 6.9 Evolution of height with time for a column collapse in fluid ($a = 0.4$)

The evolution of normalised kinetic energy with time for a column with an initial aspect ratio of 0.4 is shown in figure 6.10. It can be observed that the peak kinetic energy is attained later in the submerged condition than the dry collapse. This can be attributed to the time required to overcome the negative pore pressure generated during the shear along the fracture surface. For short columns the critical time τ_c is controlled by the vertical kinetic energy. The amount of kinetic energy in submerged case is significantly lower than the dry condition. Also, the potential energy evolution (see figure 6.11) shows a significant influence of the hydrodynamic forces on the amount of material destabilised during the collapse. The drag forces reduces and slows down the amount of material that undergo collapse resulting in shorter run-out distance for short columns.

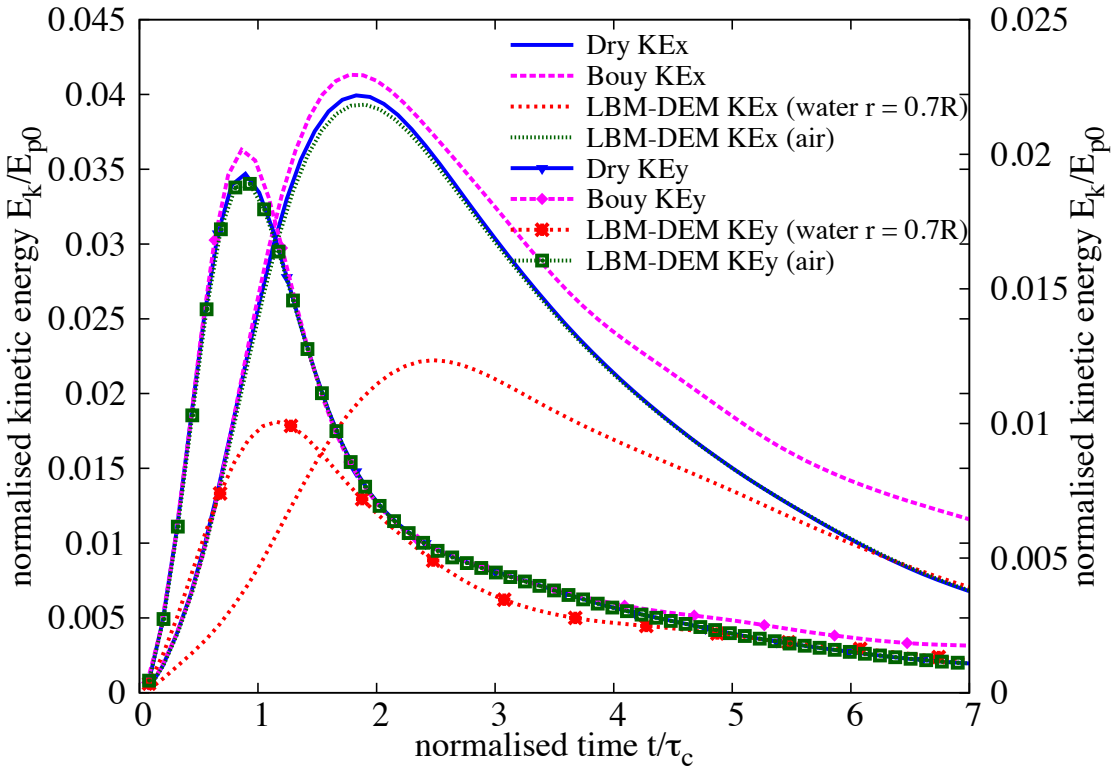
Snapshots of the flow evolution of a granular column collapse with an initial aspect ratio of 4 is shown in figure 6.12. For a tall column, the collapse mechanism change. The entire column is involved in the collapse. The height of the static region, which is below the fracture surface, is shorter than the total height of the column. This results in a free-fall of grains above the fracture surface. As the grains experience free-fall they interact with the surrounding fluid. However, no vortices are observed during the initial stage of collapse. In the second phase, when the grains reach the base, the vertical acceleration gained during the free-fall is converted to horizontal kinetic energy. As the grains are ejected horizontally, the free surface of the granular mass interacts with the fluid resulting in formation of the turbulent vortices. Unlike short columns, these vortices have significant influence on the mass distribution along the run-out. Heaps of granular material can be observed in front of each vortices. The number of vortices formed during a collapse is found to be proportional to the amount of material destabilised, i.e., the length of free-surface interacting with the fluid influences the number of vortices generated during the collapse. The reappearance of force chains at $t = 6\tau_c$ & $8\tau_c$ indicates the granular mass is consolidating resulting in an increase in the shear strength.

The time evolution of the run-out and height of a tall column ($a=4$) is presented in figure 6.13 and figure 6.14, respectively. Similar to the short column, the run-out observed in the dry condition is much longer than that observed in submerged condition. Also, the evolution of run-out is slower in case of submerged condition, which indicates the influence drag force on the run-out evolution. The height of the column is significantly affected by the hydrodynamic forces (see figures 6.14 and 6.15), which reduces the amount of material destabilised during collapse.

The evolution of kinetic energies with time for aspect ratio 4 is presented in figure 6.16. Even during the free-fall stage, the peak vertical energy is delayed in the case of fluid, which shows the influence of the viscosity on the flow evolution. Almost half of the kinetic energy that is available in the case of dry granular collapse is dissipated due to the drag force experienced by



(a) Evolution of the total kinetic energy



(b) Evolution of horizontal and vertical kinetic energies

Figure 6.10 Evolution of kinetic energies with time for a granular column collapse in fluid ($a = 0.4$)

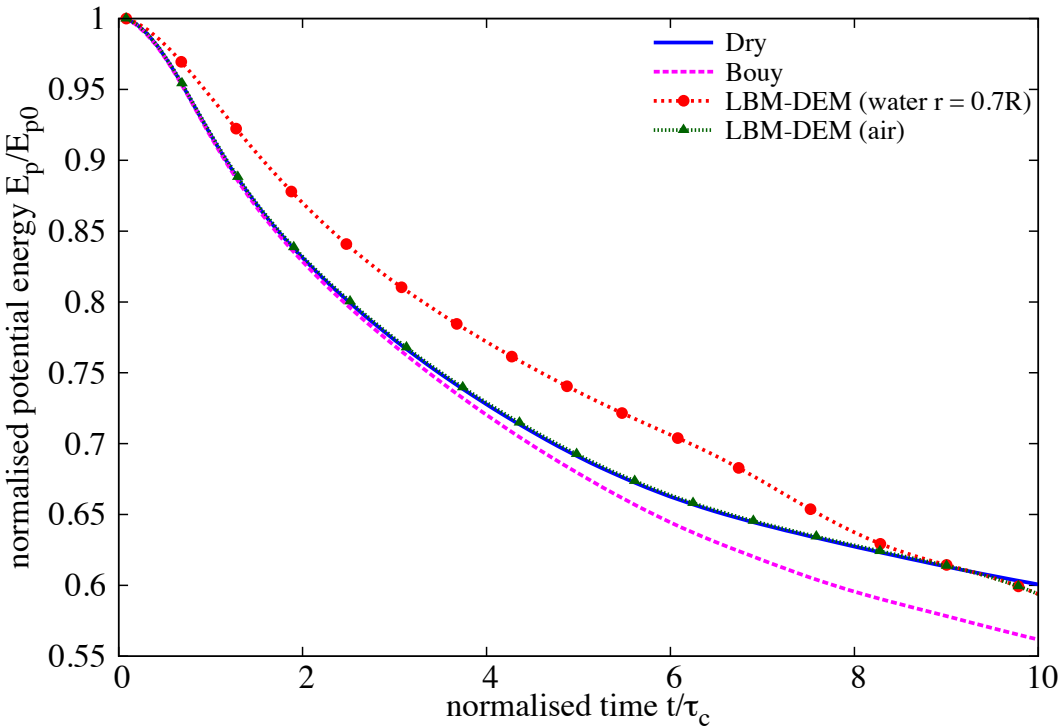


Figure 6.11 Evolution of the potential energy with time for a granular column collapse in fluid ($a = 0.4$)

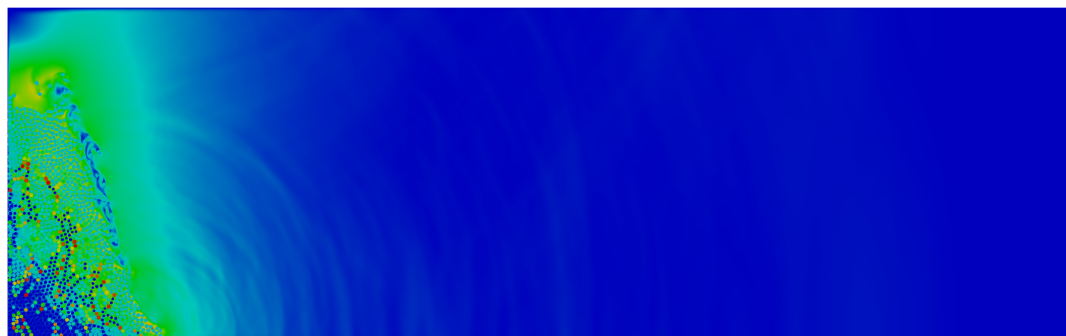
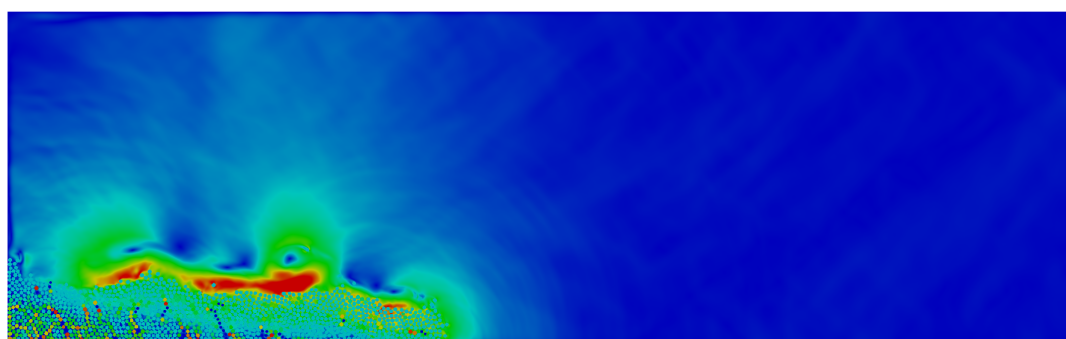
35 the grains. This shows that the influence of viscous drag on the run-out evolution is significantly
36 higher than the effect of lubrication.

1 The initial aspect ratio of the column is varied from 0.2 to 6. The final run-out distance as
2 a function of the initial aspect ratio of the column is presented in figure 6.17. For all aspect
3 ratios, the run-out observed in the dry case is significantly higher than the submerged condition.
4 For short columns, the run-out distance is found to have a linear relationship with the initial
5 aspect ratio of the column. A power law relation is observed between the run-out and the initial
6 aspect ratio of the column.

$$\frac{L_f - L_0}{L_0} \propto \begin{cases} a, & a \lesssim 2.7 \\ a^{2/3}, & a \gtrsim 2.7 \end{cases} \quad (6.5)$$

1
2
3

6.2.4 Effect of permeability

 $t = 0\tau_c$  $t = 1\tau_c$  $t = 3\tau_c$

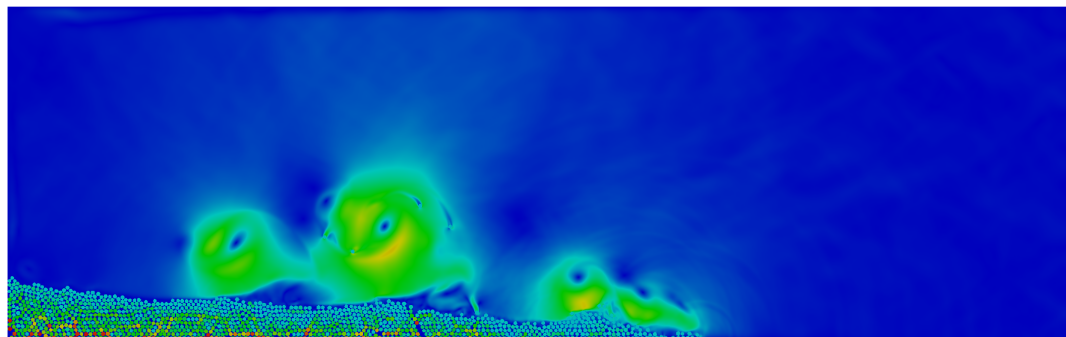
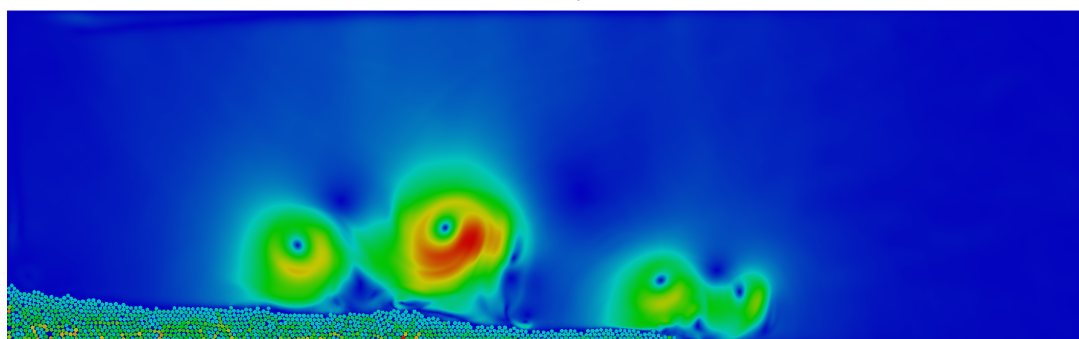
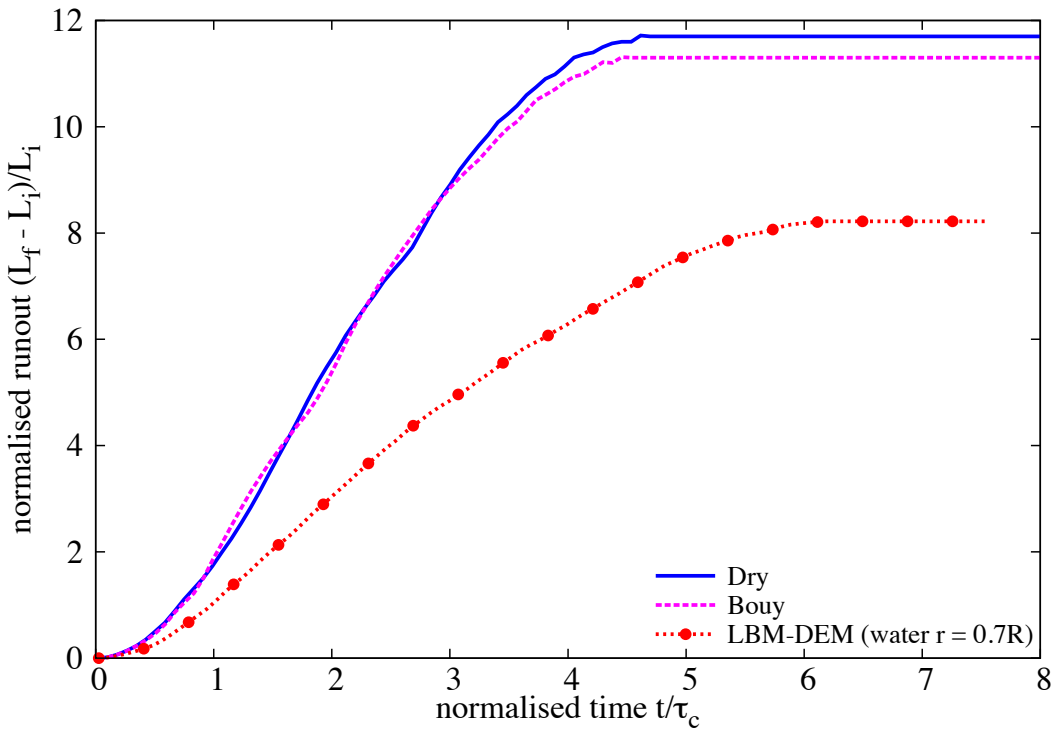
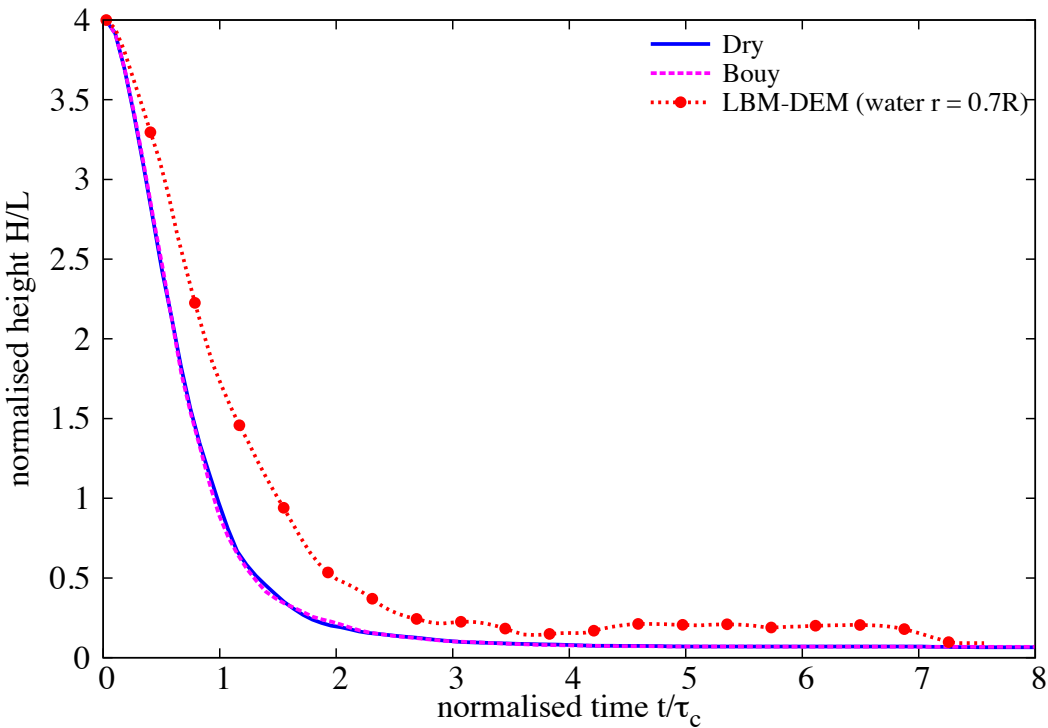
 $t = 6\tau_c$  $t = 8\tau_c$

Figure 6.12 Flow evolution of a granular column collapse in fluid ($a = 4$). Shows the velocity profile of fluid due to interaction with the grains (red - higher velocity).

Figure 6.13 Evolution of run-out for a column collapse in fluid ($a = 4$)Figure 6.14 Evolution of height with time for a column collapse in fluid ($a = 4$)

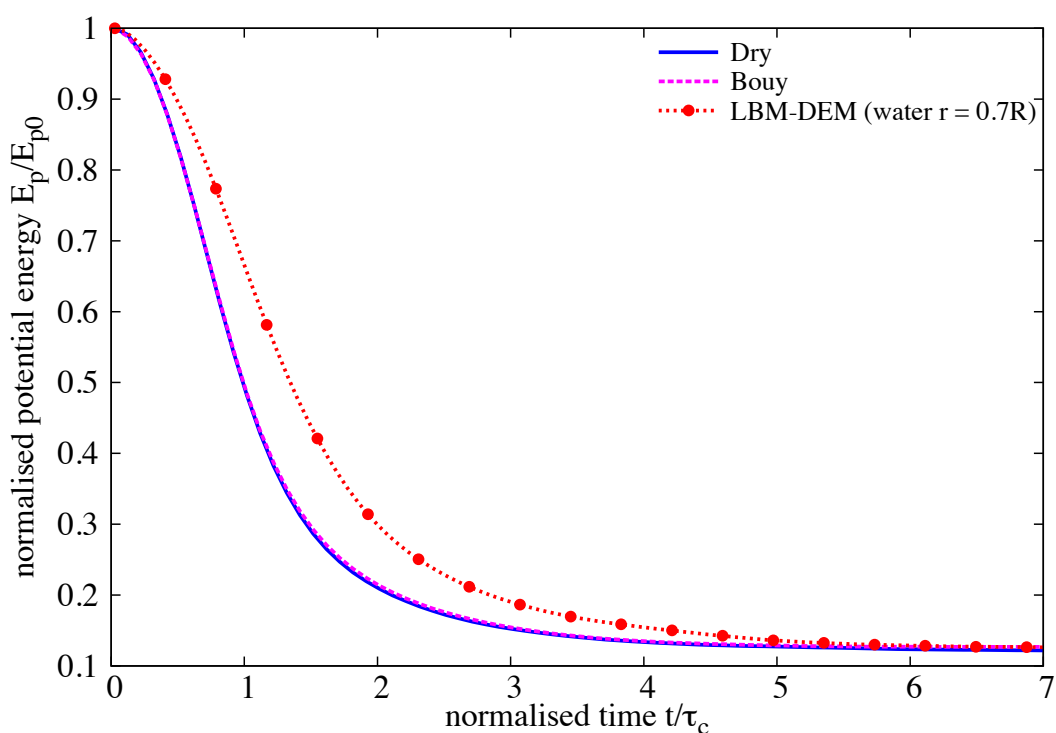
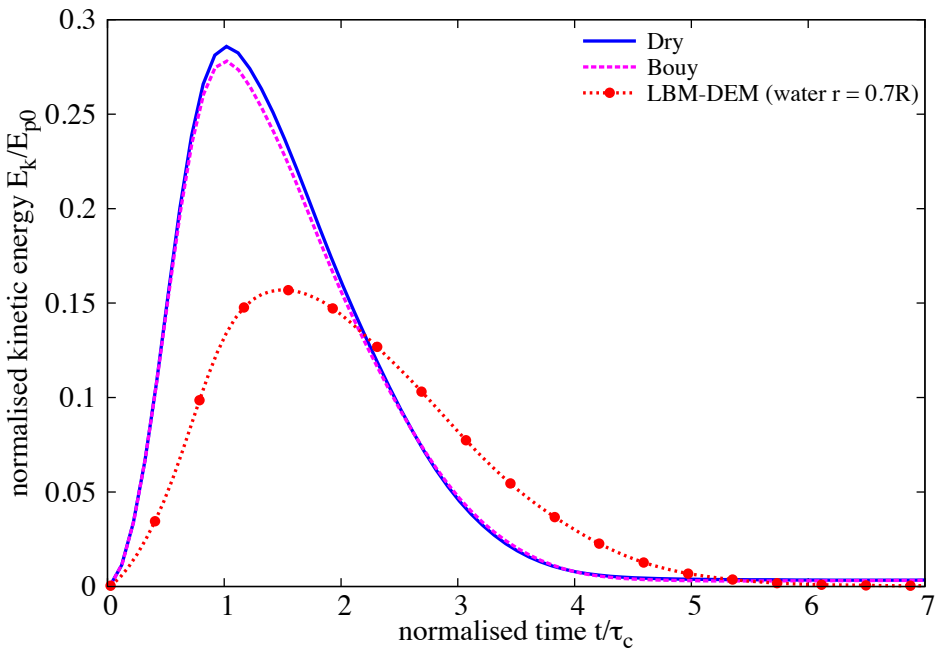
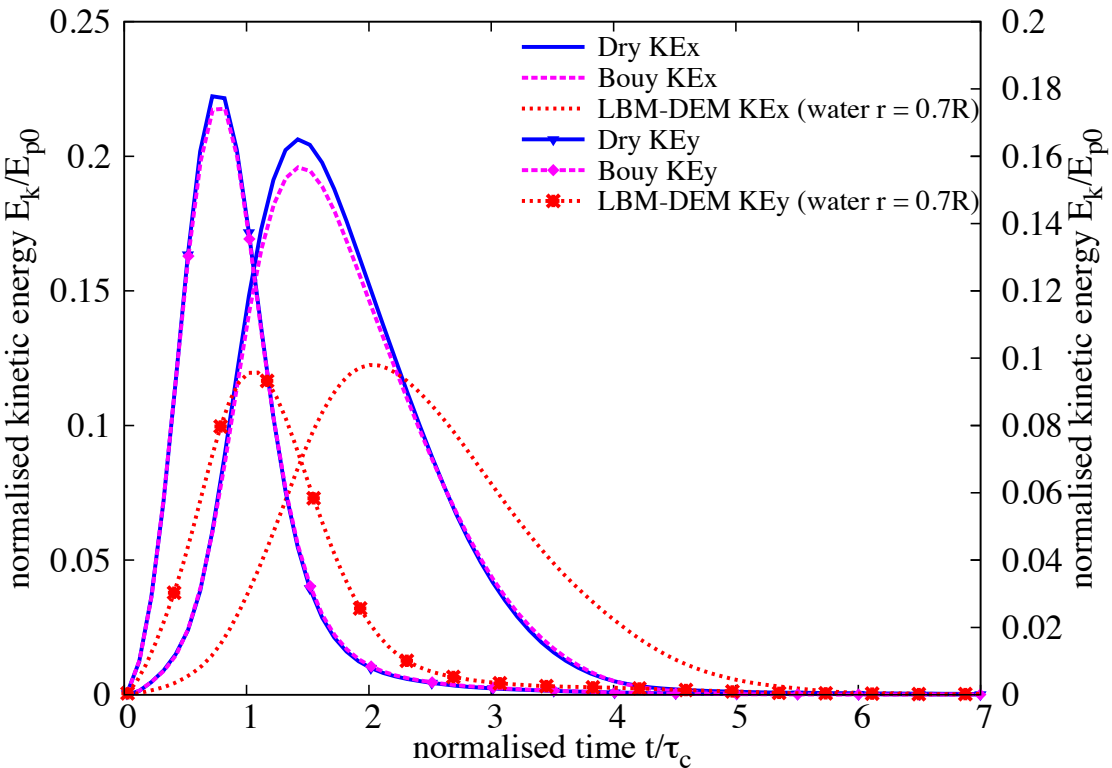


Figure 6.15 Evolution of the potential energy with time for a granular column collapse in fluid ($a = 4$)



(a) Evolution of the total kinetic energy



(b) Evolution of horizontal and vertical kinetic energies

Figure 6.16 Evolution of kinetic energies with time for a granular column collapse in fluid ($a = 4$)

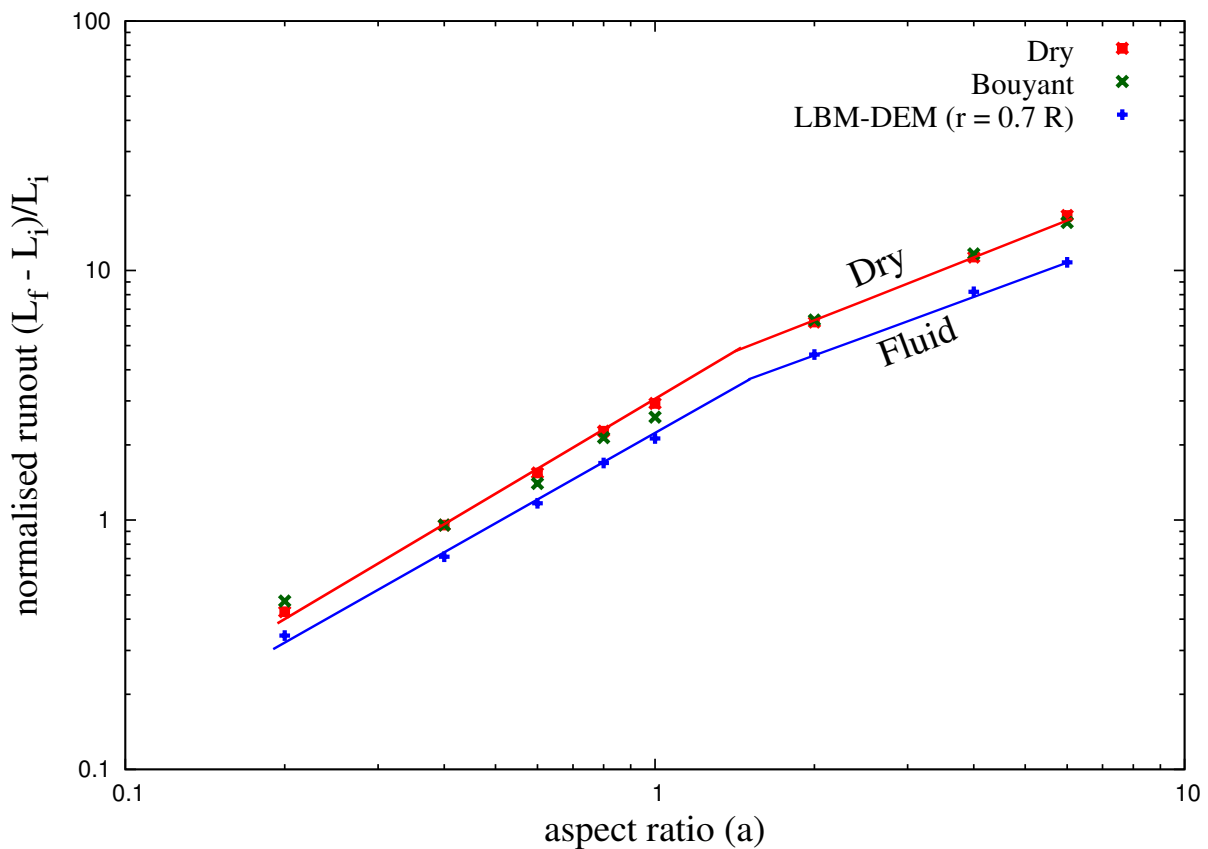


Figure 6.17 Normalised final run-out distance for columns with different initial aspect ratios. Comparison of dry and submerged granular column collapse.

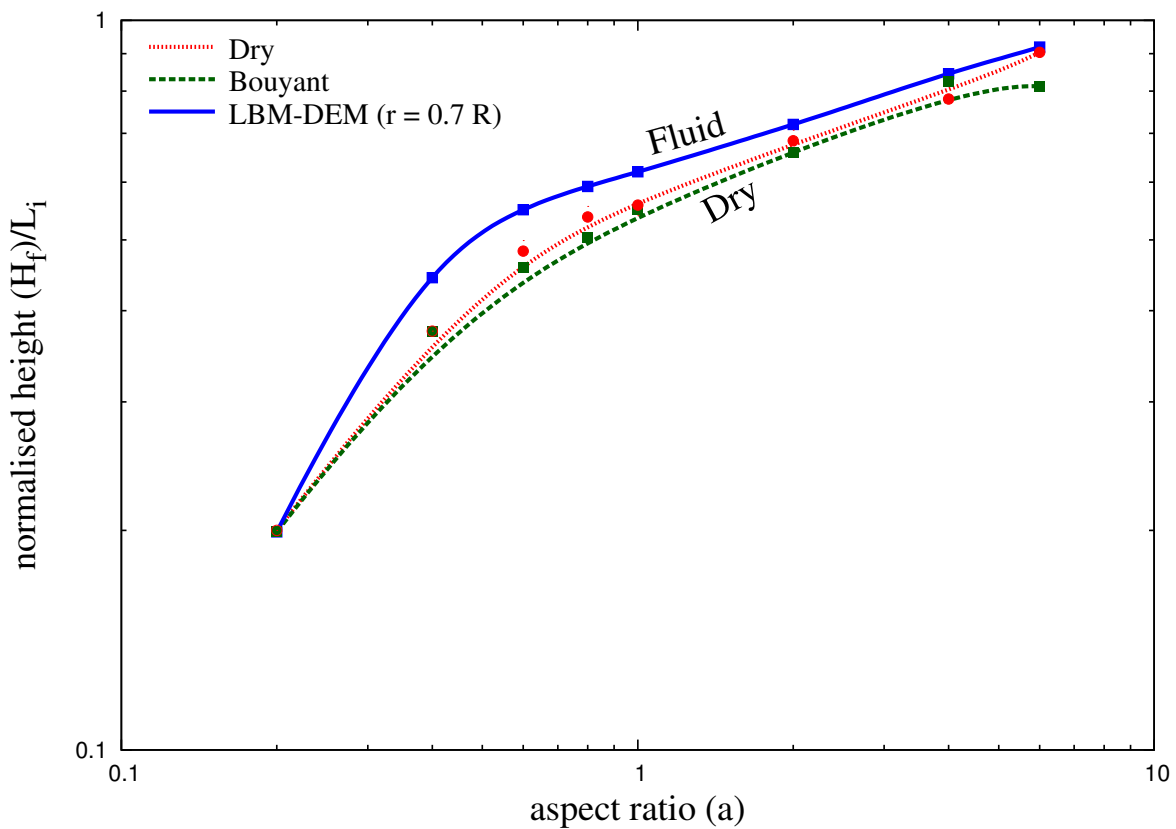


Figure 6.18 Normalised final collapse height for columns with different initial aspect ratios. Comparison of dry and submerged granular column collapse.

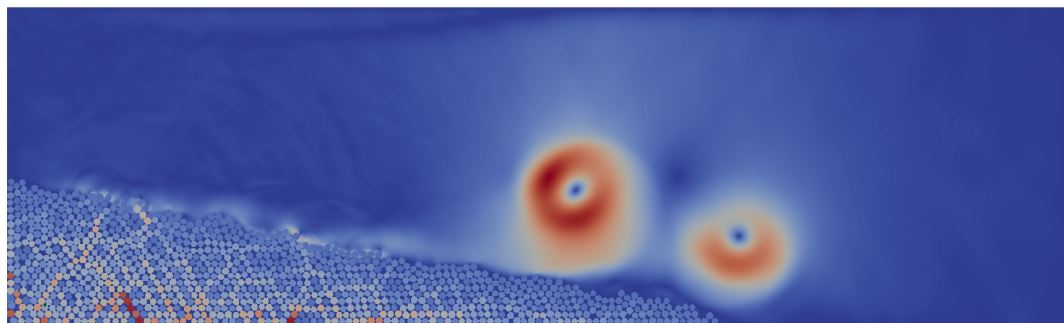
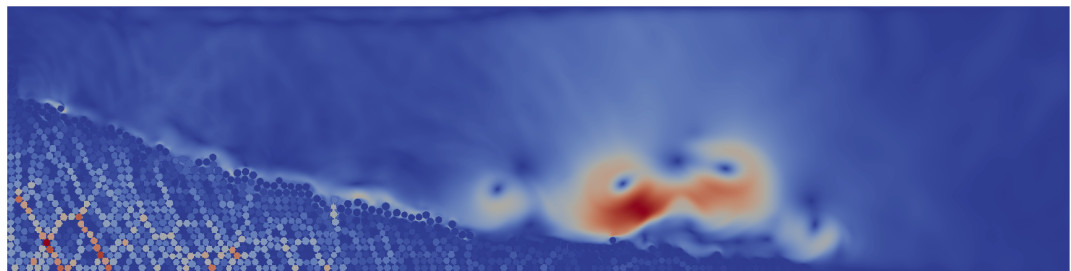
(a) High permeability ($r = 0.7 R$)(b) Low permeability ($r = 0.95 R$)

Figure 6.19 Effect of permeability on the deposit morphology of a granular column collapse in fluid ($a = 0.8$)

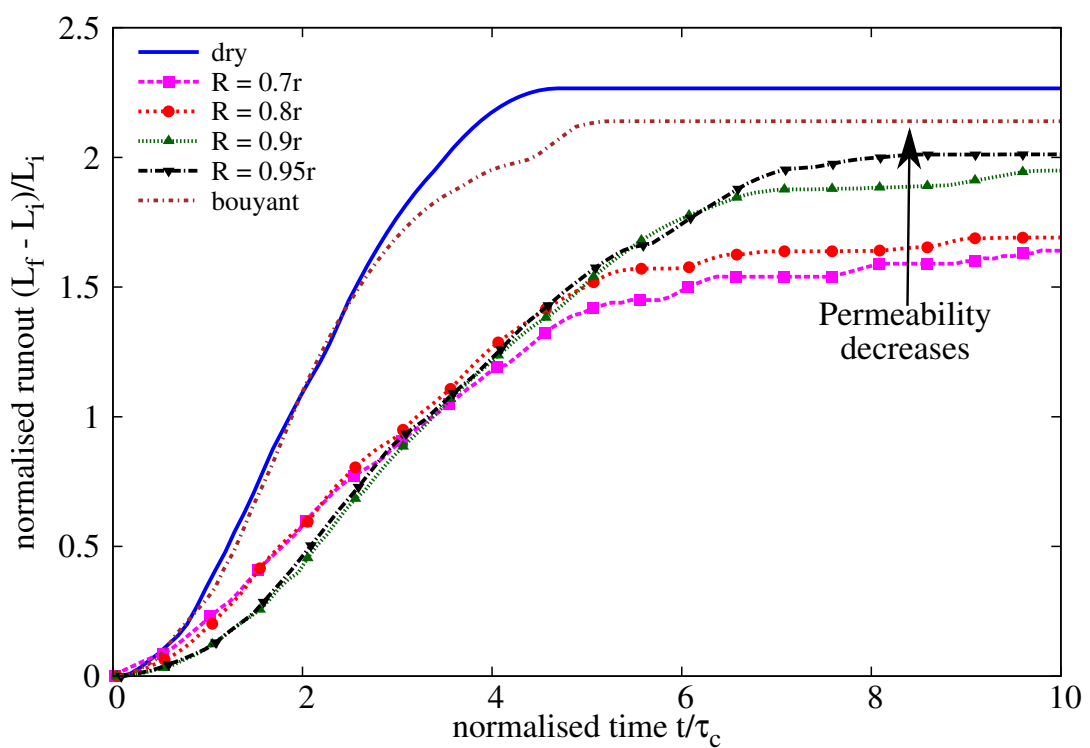
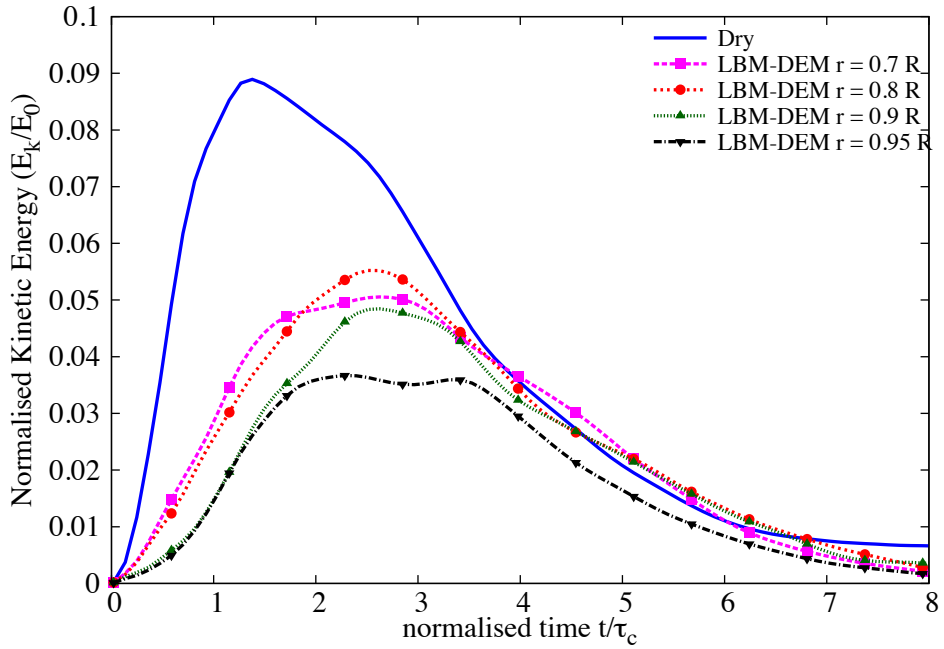
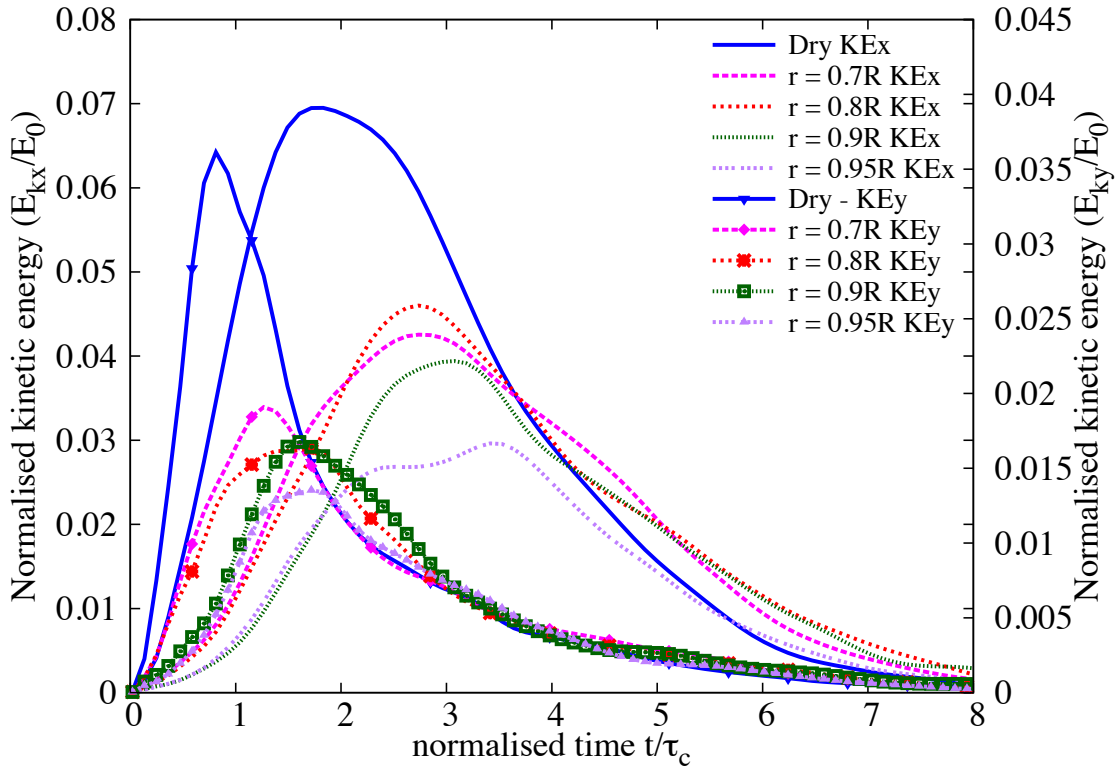


Figure 6.20 Effect of permeability on the evolution of run-out for a column collapse in fluid ($a = 0.8$)



(a) Evolution of the total kinetic energy



(b) Evolution of horizontal and vertical kinetic energies

Figure 6.21 Effect of permeability on the evolution of kinetic energies with time for a granular column collapse in fluid ($a = 0.8$)

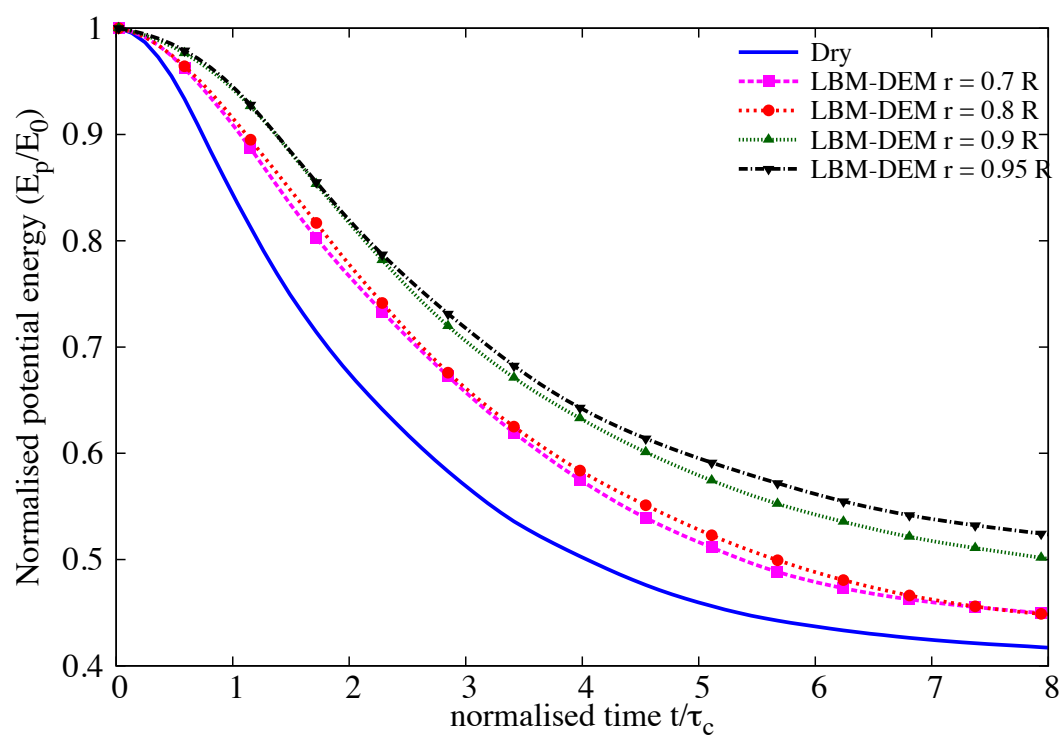


Figure 6.22 Effect of permeability on the evolution of the potential energy with time for a granular column collapse in fluid ($a = 0.8$)

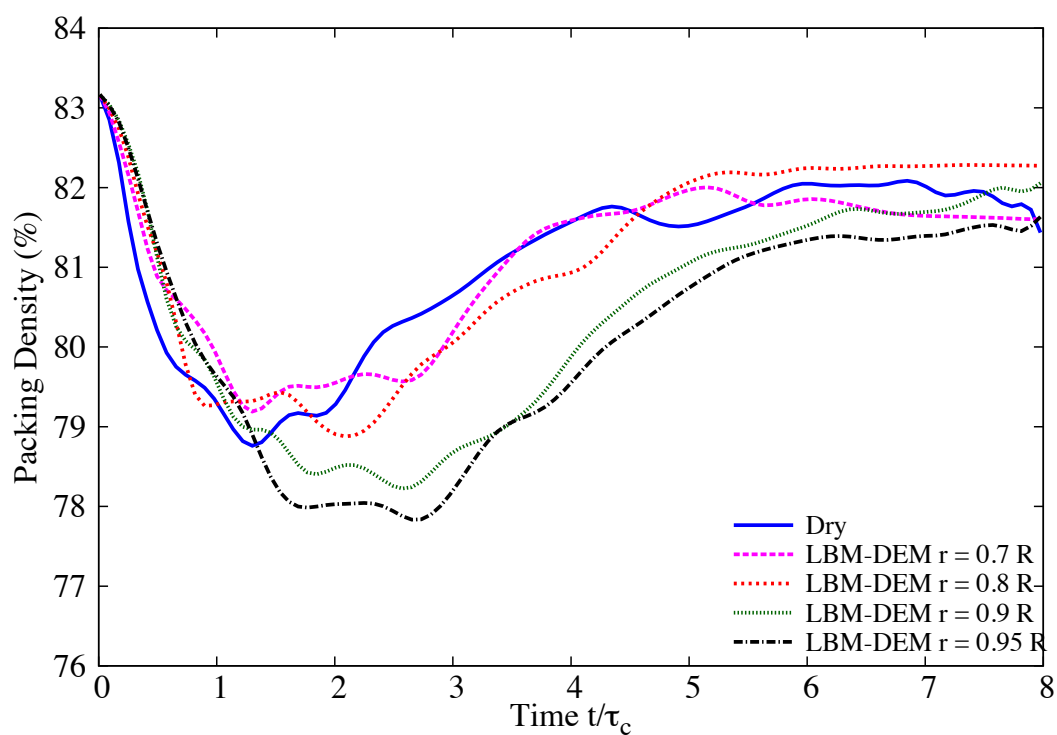


Figure 6.23 Effect of permeability on the evolution of packing density for a granular column collapse in fluid ($a = 0.8$ & dense initial packing)

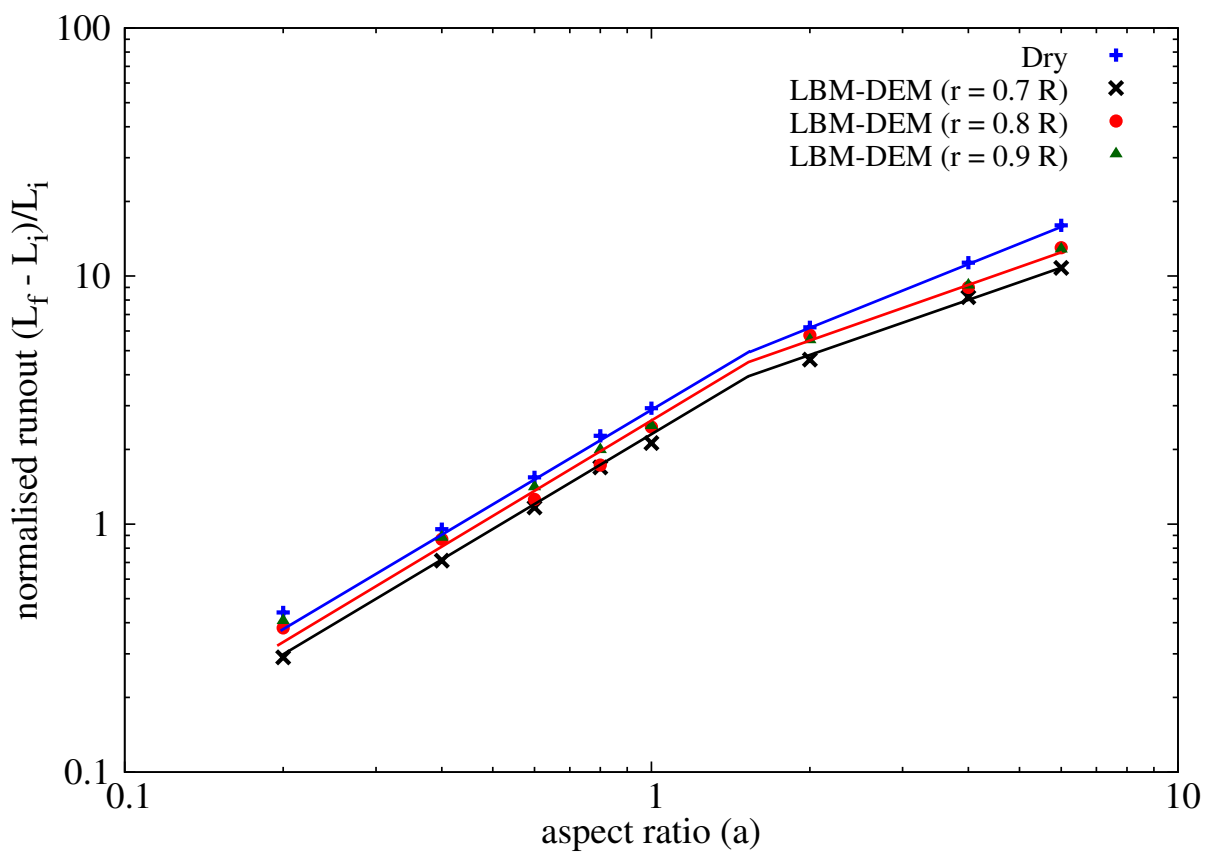


Figure 6.24 Normalised final run-out distance for columns with different initial aspect ratios. Comparison of dry and submerged granular column collapse for different hydrodynamic radius ($0.7R$, $0.8R$ and $0.9R$).

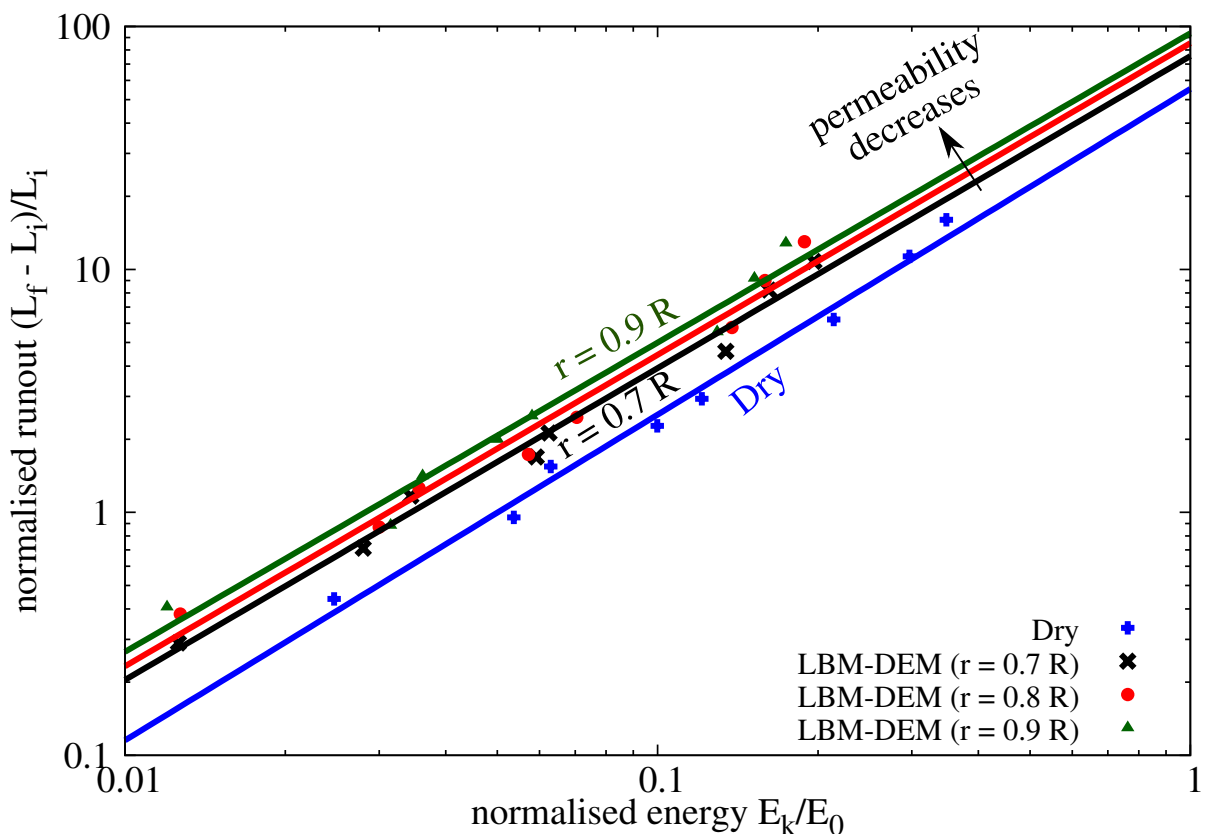


Figure 6.25 Normalised final run-out distance for columns as a function of peak kinetic energy. Comparison of dry and submerged granular column collapse for different hydrodynamic radius ($0.7R$, $0.8R$ and $0.9R$).

6.3 Submarine granular flows down incline plane

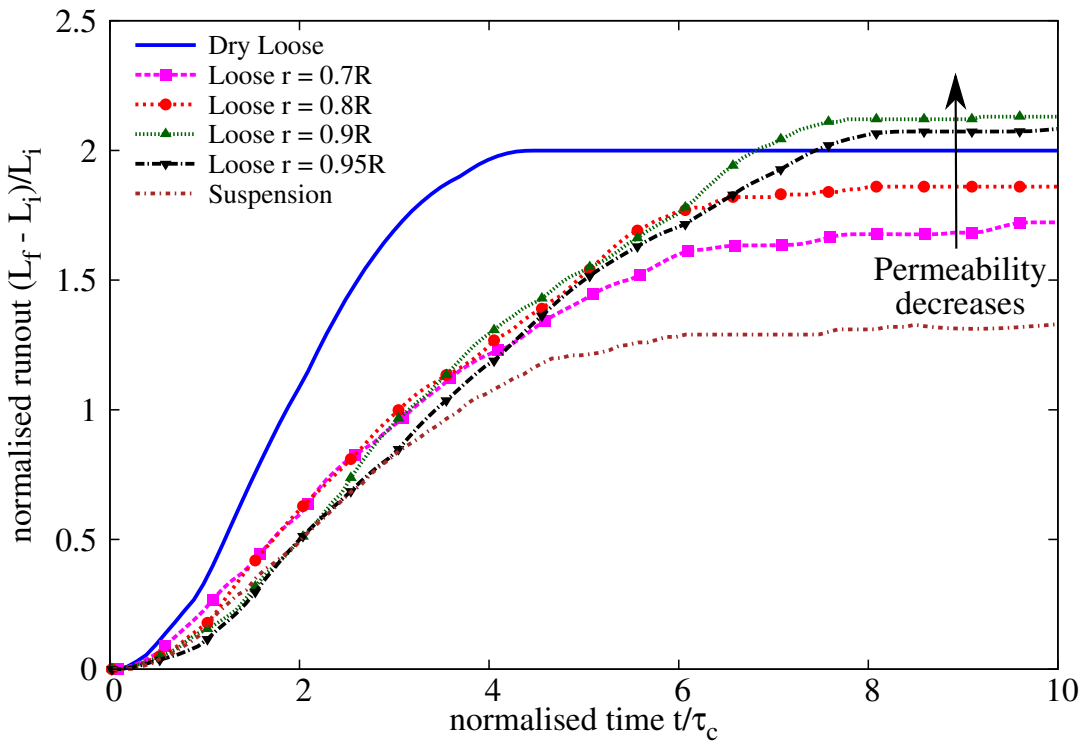


Figure 6.26 Effect of permeability on the evolution of run-out for a column collapse in fluid ($a = 0.8$ & loose packing)

6.2.5 Effect of initial packing density

6.3 Submarine granular flows down incline plane

The flow of dense granular material is a common phenomenon in engineering predictions, such as avalanches, landslides, and debris-flow modelling. Despite the huge amount of research that has gone into describing the behaviour of granular flows, a constitutive equation that describes the overall behaviour of a flowing granular material is still lacking. The initiation and propagation of submarine granular flows depend mainly on the slope, density, and quantity of the material destabilised. Although certain macroscopic models are able to capture the simple mechanical behaviours, the complex physical mechanisms that occur at the grain scale, such as hydrodynamic instabilities, the formation of clusters, collapse, and transport, have largely been ignored (Topin et al., 2011). The momentum transfer between the discrete and the continuous phases significantly affects the dynamics of the flow (Peker and Helvacı, 2007). Grain-scale

¹ description of the granular material enriches the macro-scale variables, which poorly account for the local rheology of the materials. In order to describe the mechanism of saturated and/or ² immerssed granular flows, it is important to consider both the dynamics of the solid phase and ³

(a) High permeability ($r = 0.7 R$)(b) Low permeability ($r = 0.95 R$)

Figure 6.27 Effect of permeability on the excess pore water pressure distribution for a granular column collapse in fluid ($a = 0.8$ & loose packing) at $t = \tau_c$

6.3 Submarine granular flows down incline plane

31

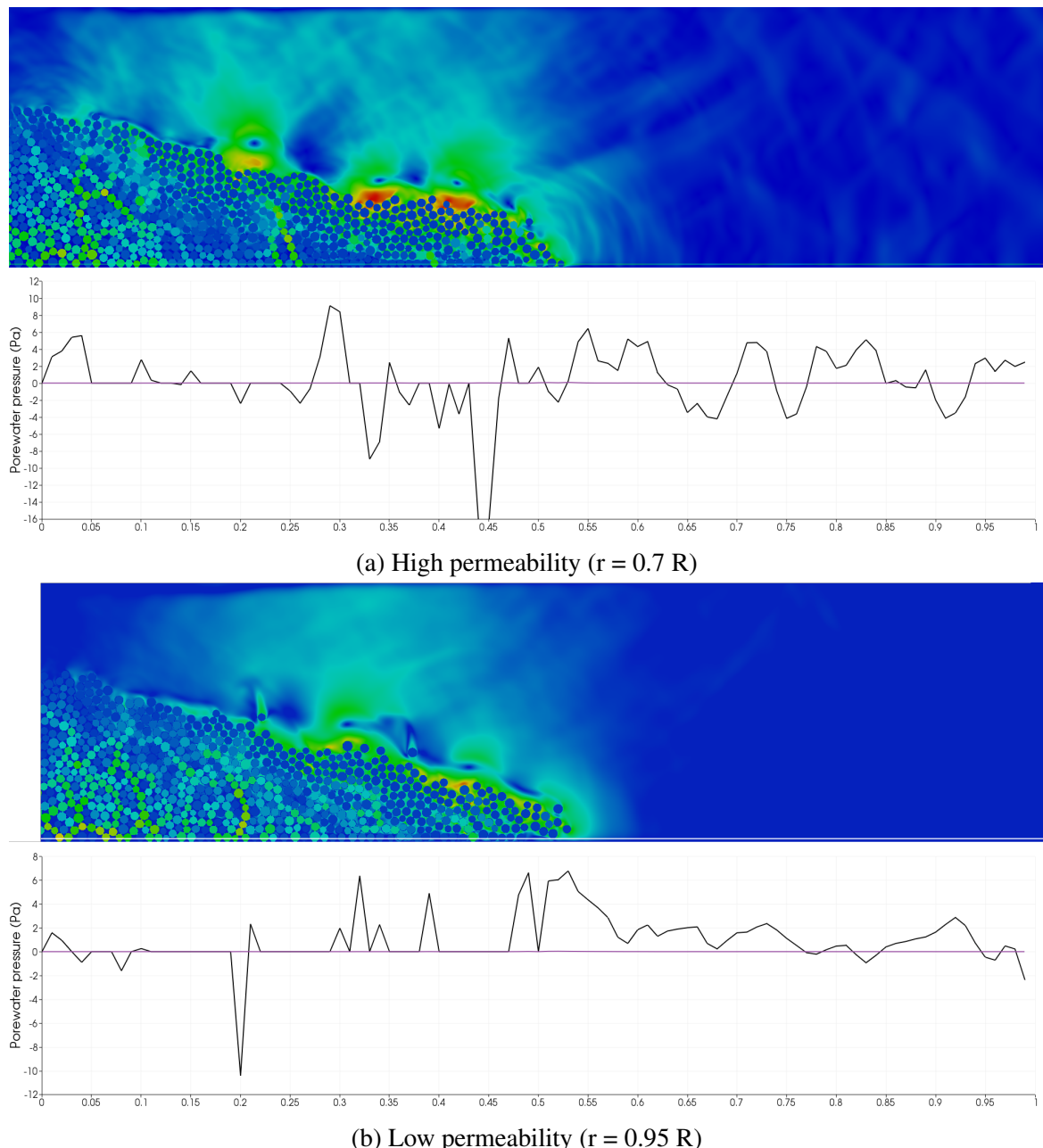


Figure 6.28 Effect of permeability on the excess pore water pressure distribution for a granular column collapse in fluid ($a = 0.8$ & loose packing) at $t = 2\tau_c$

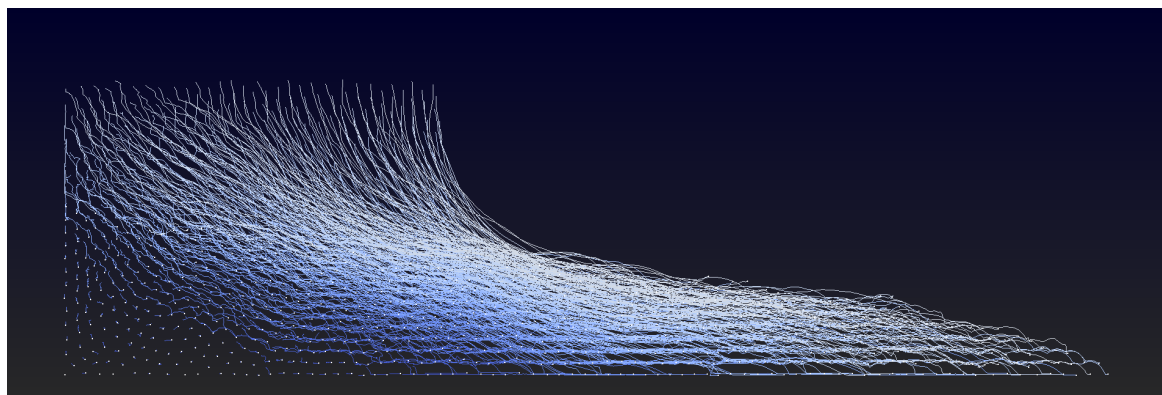
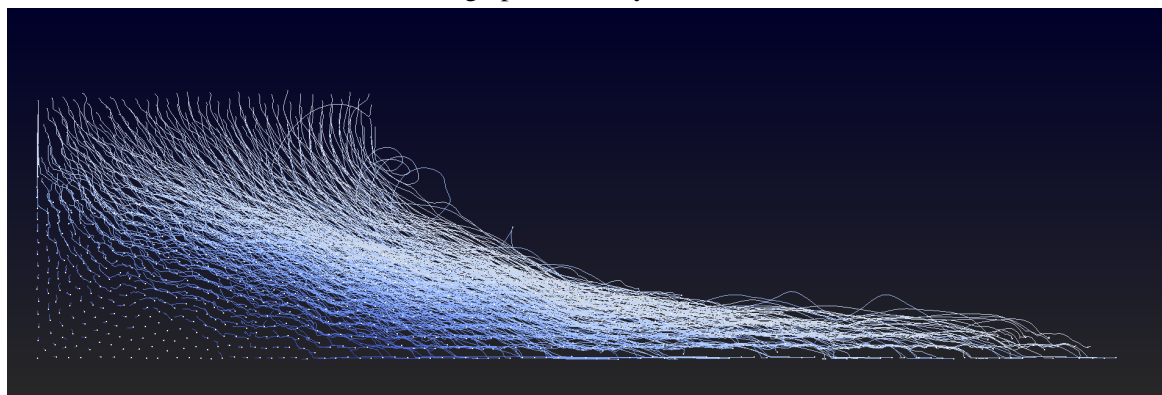
(a) High permeability ($r = 0.7 R$)(b) Low permeability ($r = 0.95 R$)

Figure 6.29 Particle tracking of the deposit morphology for a granular column collapse in fluid ($a = 0.8$ & loose packing), influence of permeability

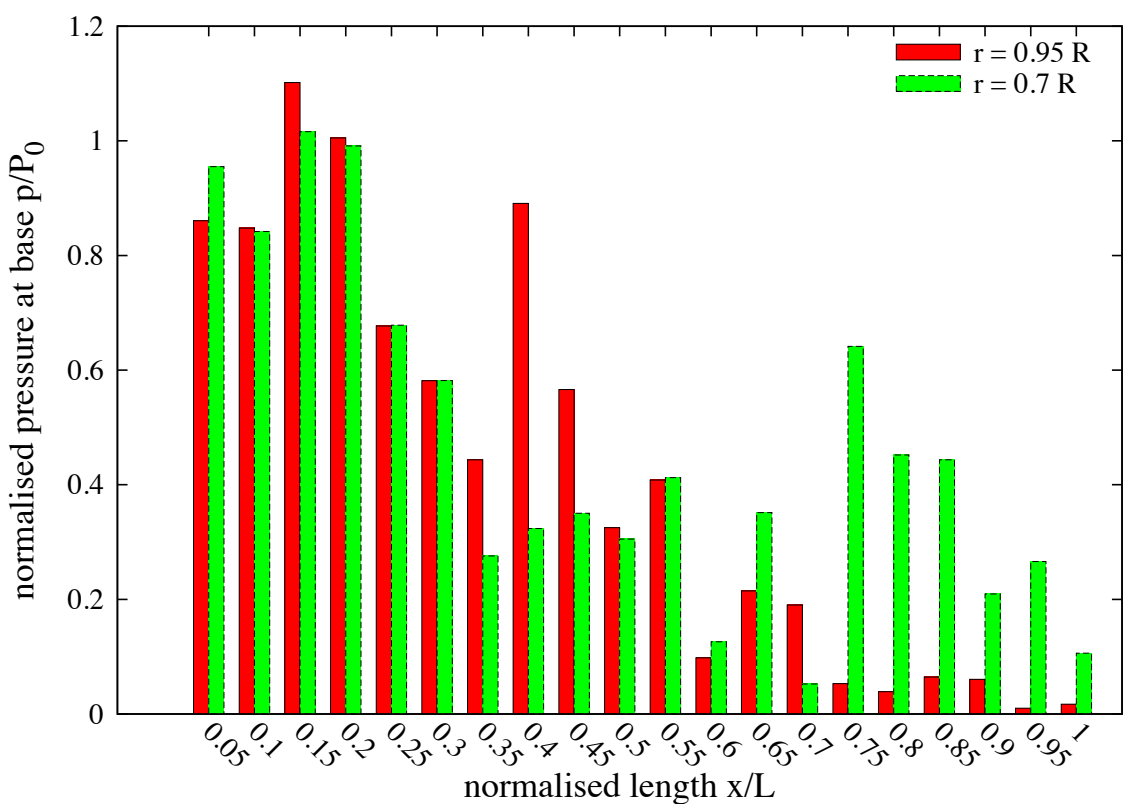
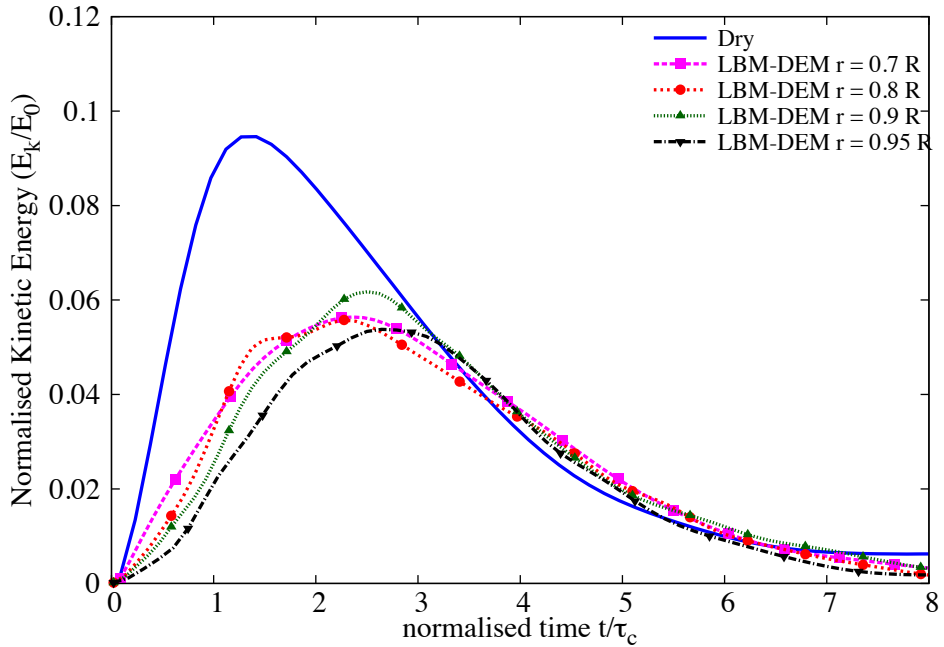
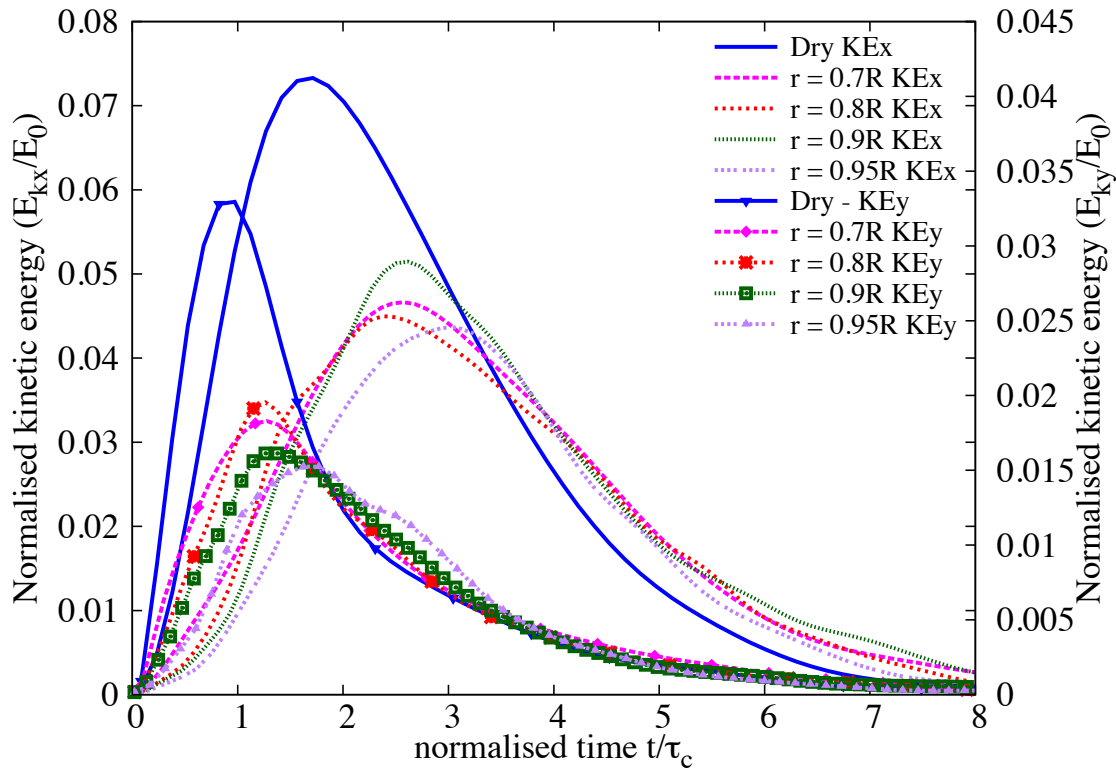


Figure 6.30 Effect of permeability on the normalised effective stress for loose initial packing at $t = \tau_c$



(a) Evolution of the total kinetic energy



(b) Evolution of horizontal and vertical kinetic energies

Figure 6.31 Effect of permeability on the evolution of kinetic energies with time for a granular column collapse in fluid ($a = 0.8$ & loose packing)

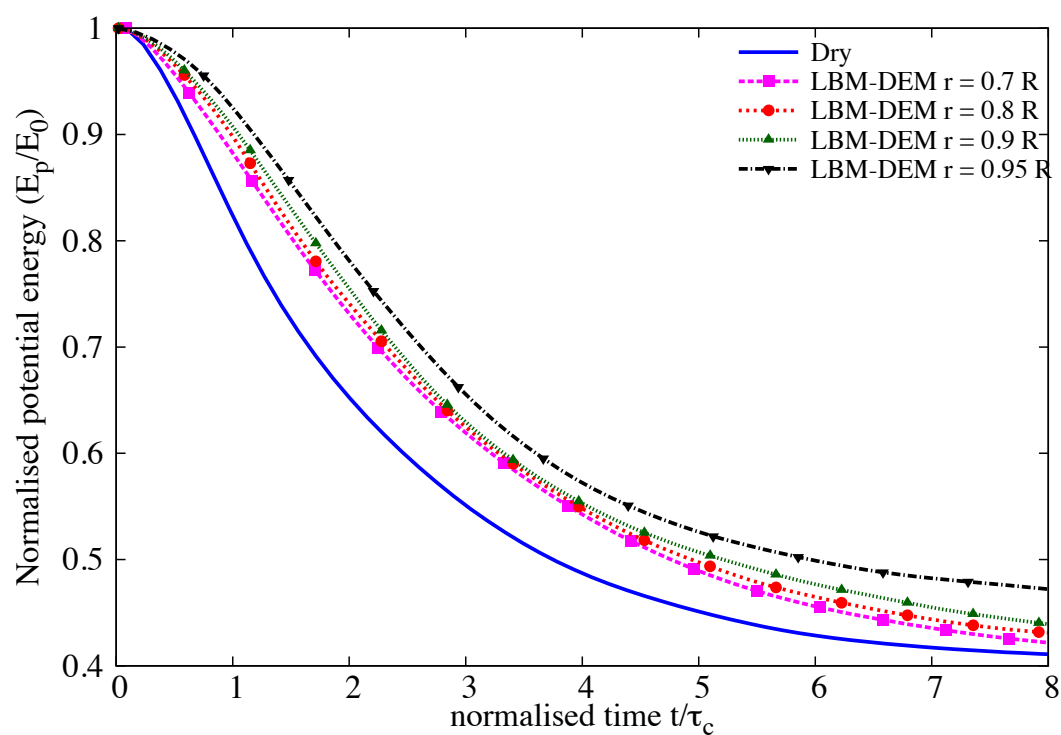


Figure 6.32 Effect of permeability on the evolution of the potential energy with time for a granular column collapse in fluid ($a = 0.8$ & loose packing)

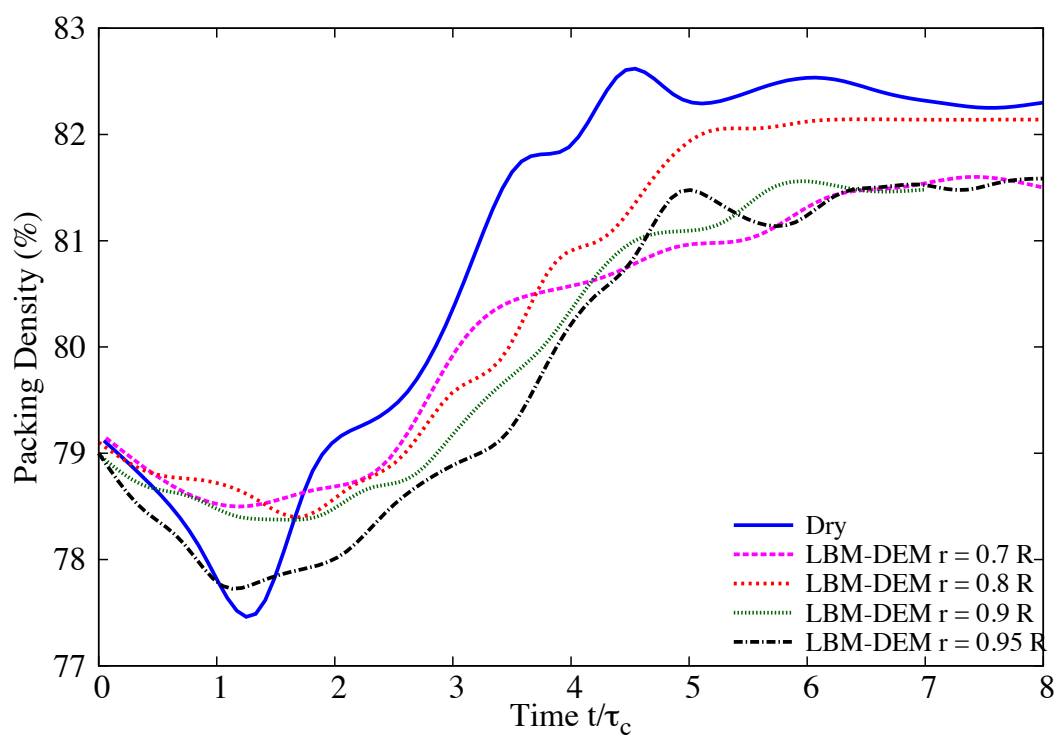
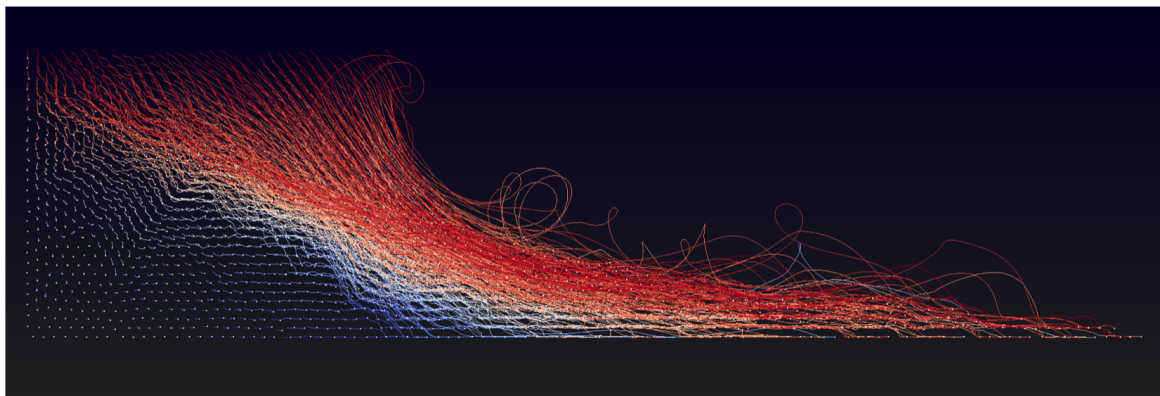
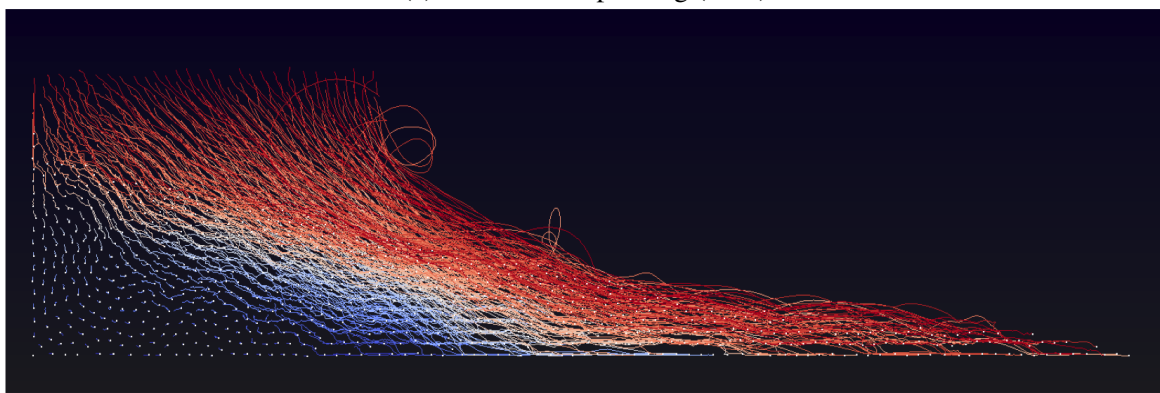


Figure 6.33 Effect of permeability on the evolution of packing density for a granular column collapse in fluid ($a = 0.8$ & loose initial packing)



(a) Dense initial packing (79%)



(b) Loose initial packing (83%)

Figure 6.34 Effect of initial density on the deposit morphology for a granular column collapse in fluid ($\alpha = 0.8$). Dense vs loose initial packing fraction.



(a) Dense initial packing (83%)



(b) Loose initial packing (79%)

Figure 6.35 Evolution of packing fraction at $t = \tau_c$ for dense and loose initial packing fraction.

the role of the ambient fluid (Denlinger and Iverson, 2001). In particular, when the solid phase reaches a high volume fraction, it is important to consider the strong heterogeneity arising from the contact forces between the grains, the drag interactions which counteract the movement of the grains, and the hydrodynamic forces that reduce the weight of the solids inducing a transition from dense compacted to a dense suspended flow (Meruane et al., 2010). The case of the collapse in presence of an interstitial fluid has been less studied. In this paper, we study the submarine granular flows in the inclined configuration. We study the effect of permeability, density and slope angle on the run-out evolution.

In this study, a 2D poly-disperse system ($d_{max}/d_{min} = 1.8$) of circular discs in fluid was used to understand the behaviour of granular flows on inclined planes (see ??). The soil column was modelled using 1000 discs of density 2650 kg m^{-3} and a contact friction angle of 26° . The collapse of the column was simulated inside a fluid with a density of 1000 kg m^{-3} and a kinematic viscosity of $1 \times 10^{-6} \text{ m}^2 \text{ s}^{-1}$. The choice of a 2D geometry has the advantage of cheaper computational effort than a 3D case, making it feasible to simulate very large systems. A granular column of aspect ratio ‘a’ of 0.8 was used. A hydrodynamic radius $r = 0.9R$ was adopted during the LBM computations. Dry analyses were also performed to study the effect of hydrodynamic forces on the run-out distance.

6.3.1 Effect of initial density

The morphology of the granular deposits in fluid is shown to be mainly controlled by the initial volume fraction of the granular mass and not by the aspect ratio of the column (Pailha et al., 2008; Rondon et al., 2011). In order to understand the influence of the initial packing density on the run-out behaviour, a dense sand column (initial packing density, $\Phi = 83\%$) and a loose sand column ($\Phi = 79\%$) were used. The granular columns collapse and flow down slopes of varying inclinations (2.5° , 5° and 7.5°).

The evolution of run-out distances for a dense sand column with time in dry and submerged conditions for varying slope inclinations are presented in figure 6.36. The run-out distance is longer in submerged condition than the dry condition for a flow on a horizontal surface. However, with increase in the slope angle the run-out in the fluid decreases.

Dense granular columns in fluid take a longer time to collapse and flow, due to the development of large negative pore-pressure, as the dense granular material dilates during the initial phase of the flow. The morphology of dense granular flows down slopes of varying inclinations at the critical time ($t = \tau_c = \sqrt{H/g}$, when the flow is fully mobilised) are shown in figure 6.38.

It can be seen that the viscous drag on the dense column tend to predominate over the influence of hydroplaning on the run-out behaviour. This influence can be observed in the smaller peak kinetic energy for granular column in fluid compared to its dry counterpart

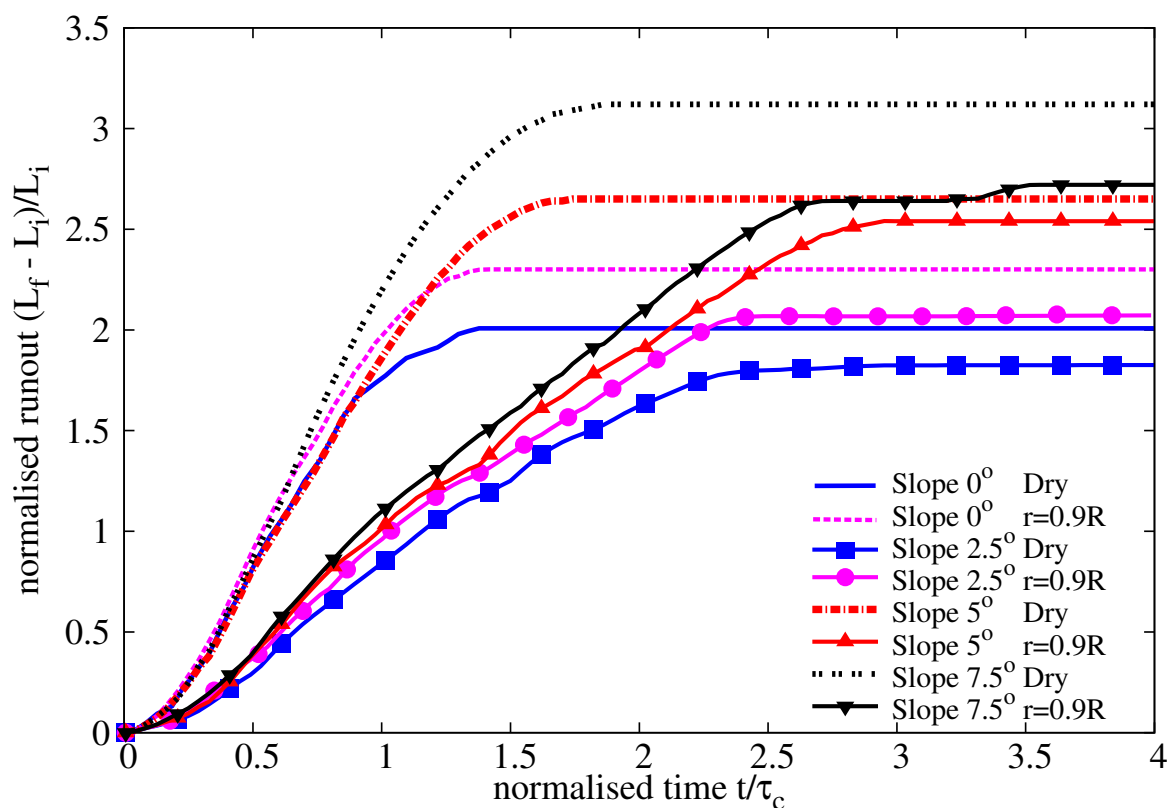


Figure 6.36 Evolution of run-out with time (dense)

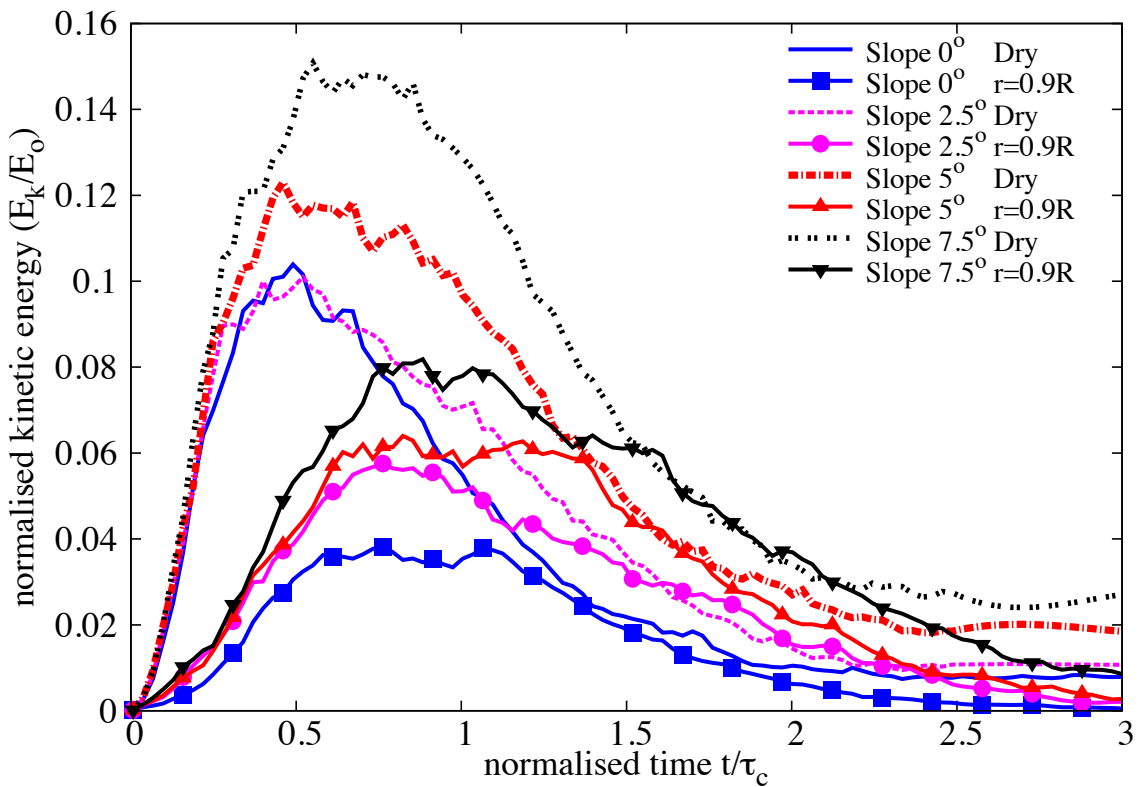
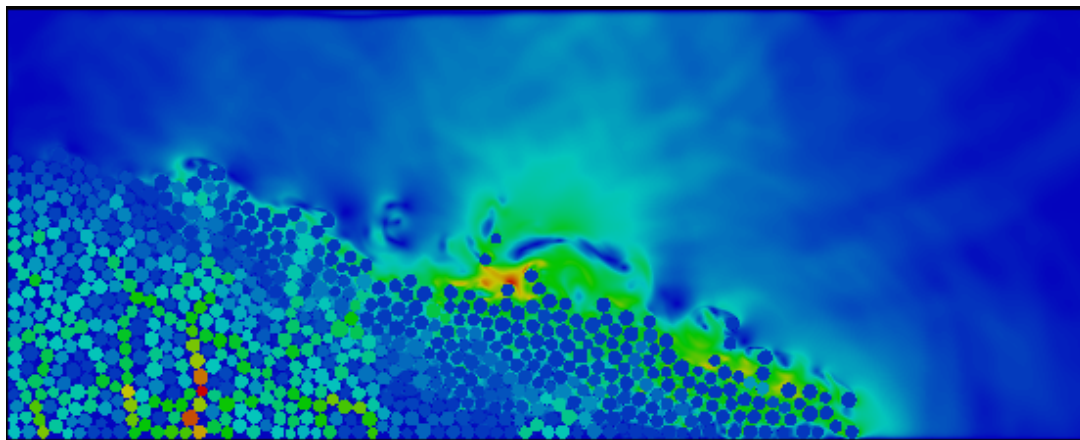


Figure 6.37 Evolution of Kinetic Energy with time (dense case)

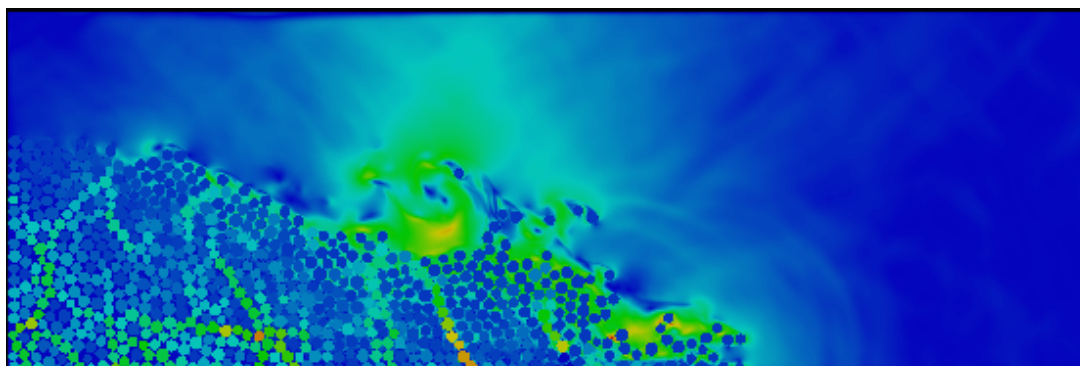
(see Figure 6.37). With increase in slope angle, the volume of material that dilates increases. This results in large negative pore pressures and more viscous drag on the granular material. Hence, the difference in the run-out between the dry and the submerged condition, for a dense granular assembly, increases with increase in the slope angle.

In contrast to the dense granular columns, the loose granular columns (relative density $I_D = 30\%$) show longer run-out distance in immersed conditions (see Figure 6.39). The run-out distance in fluid increases with increase in the slope angle compared to the dry cases. Loose granular material tends to entrain more water at the base of the flow front, creating a lubricating surface, which causes longer run-out distance (see Figure 6.40). The hydroplaning effect causes an increase in the velocity the loose condition in comparison with the dense condition (see Figure 6.41).

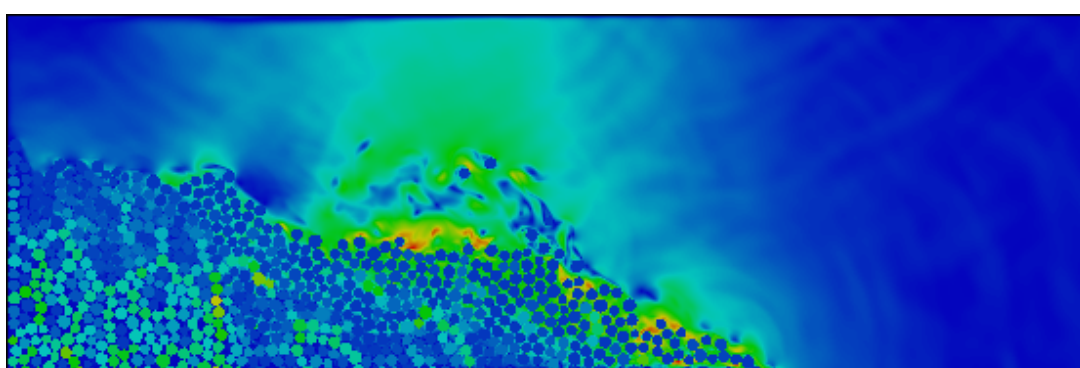
The evolution of packing density (see Figure 6.42) shows that dense and the loose conditions reach similar packing density. This indicates that the dense granular column dilates more and is susceptible to higher viscous drag forces. Where as in the loose condition, a positive pore-pressure is observed at the base of the flow, indicating entrainment of water at the base, i.e. hydroplaning resulting in longer run-out distance.



(a) Slope 2.5



(b) Slope 5.0



(c) Slope 7.5

Figure 6.38 Flow morphology at critical time for different slope angles (dense)

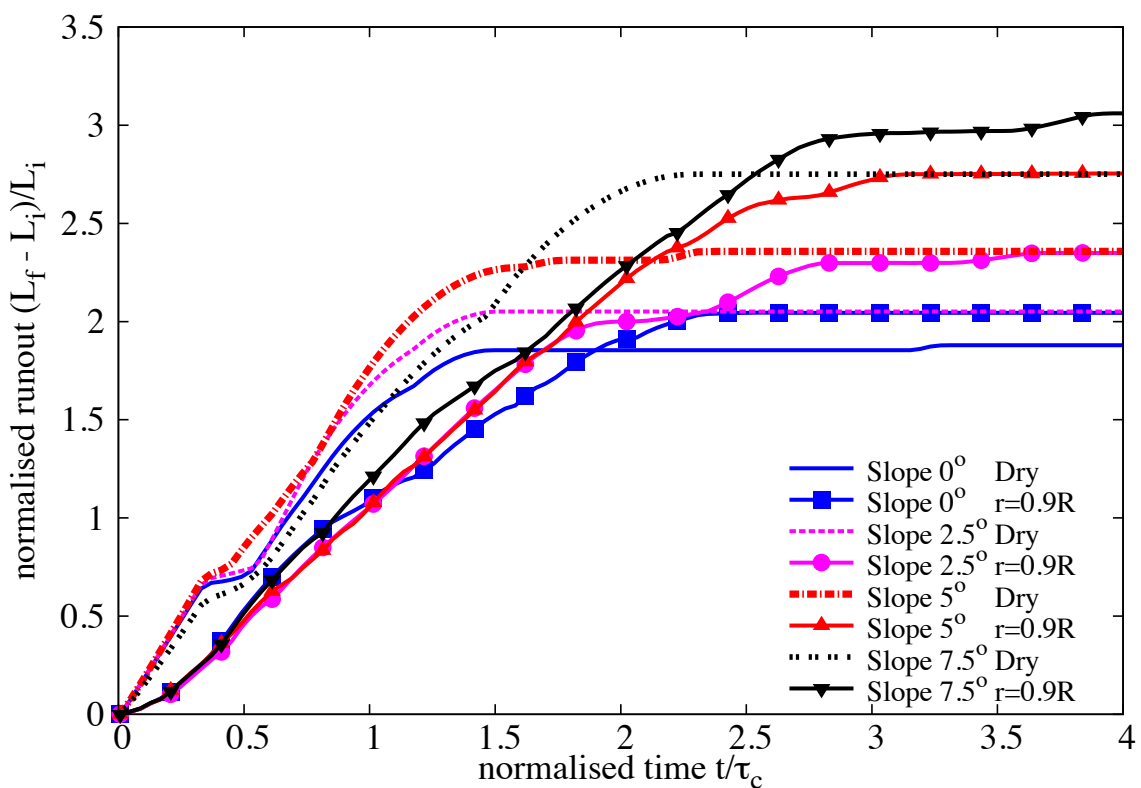
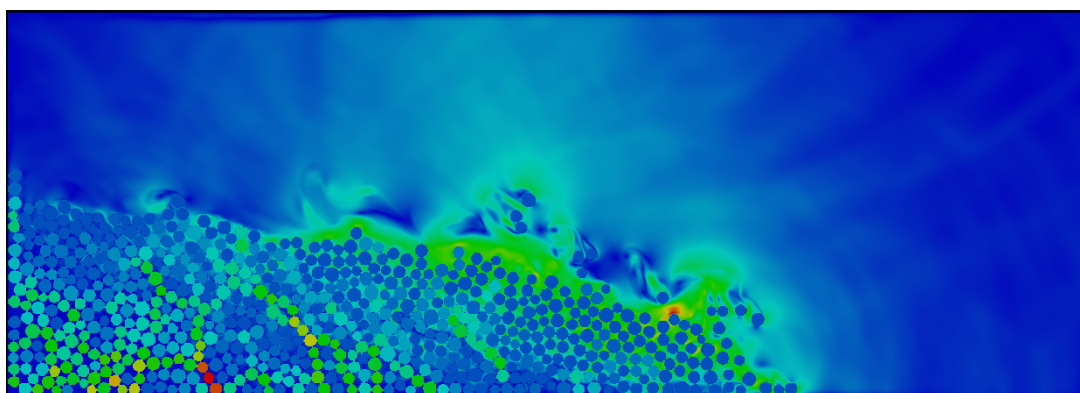
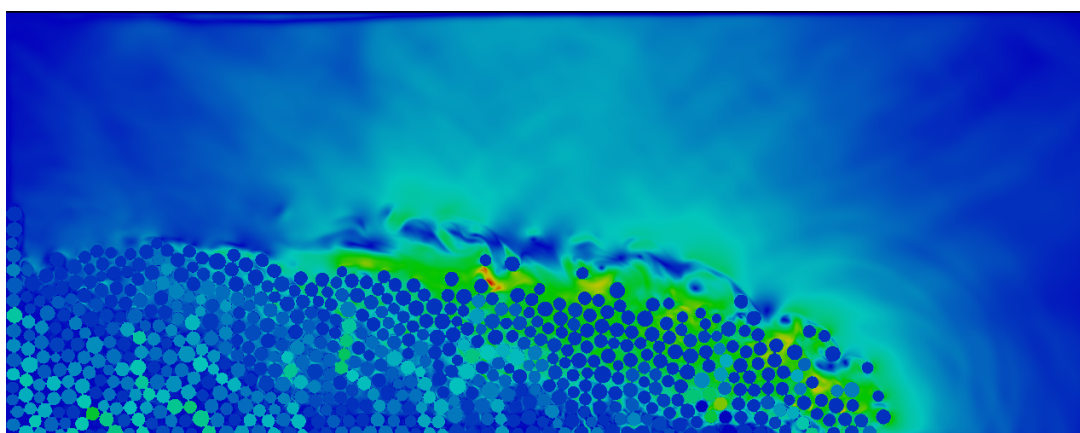


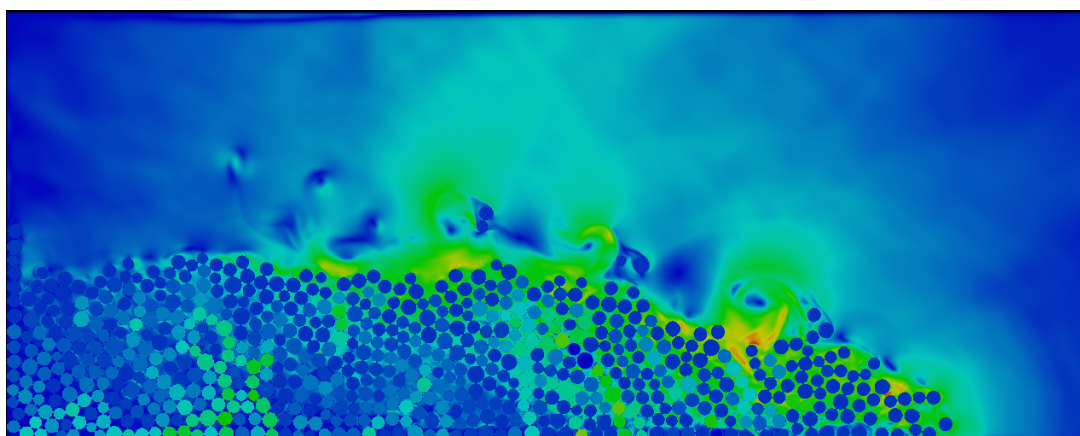
Figure 6.39 Evolution of run-out with time (loose)



(a) Slope 2.5



(b) Slope 5.0



(c) Slope 7.5

Figure 6.40 Flow morphology at critical time for different slope angles (loose)

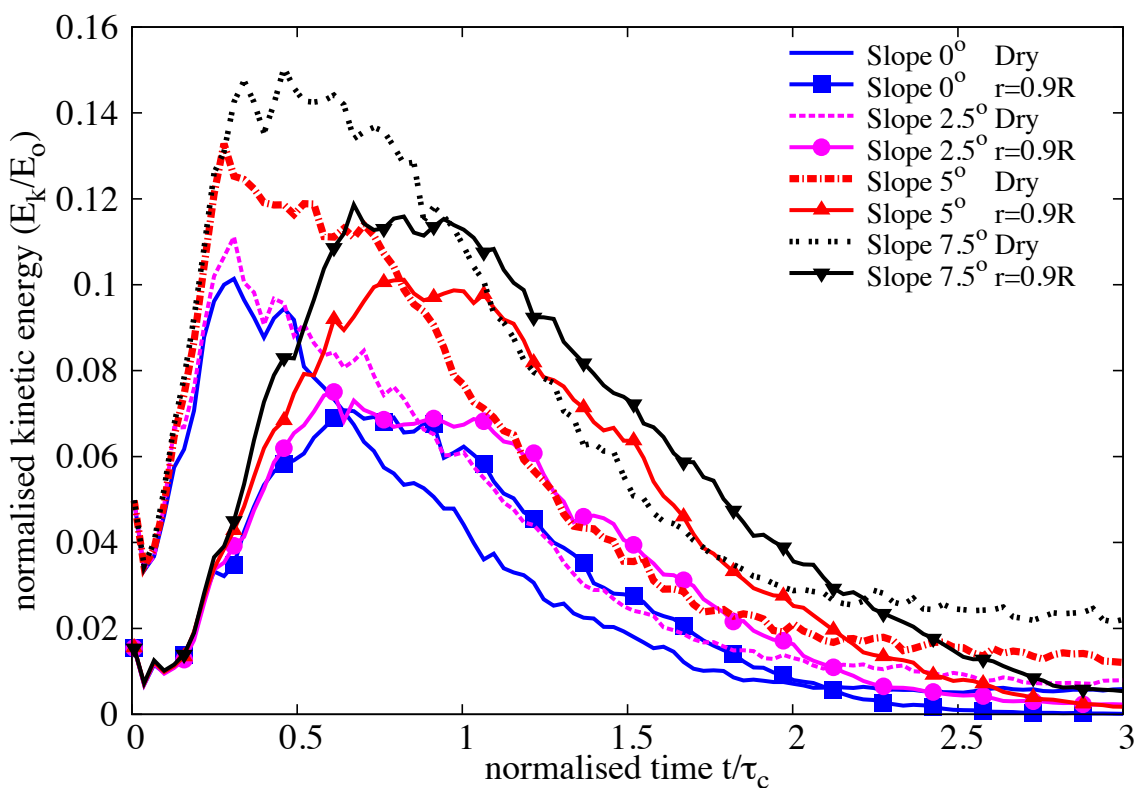


Figure 6.41 Evolution of Kinetic Energy with time (loose)

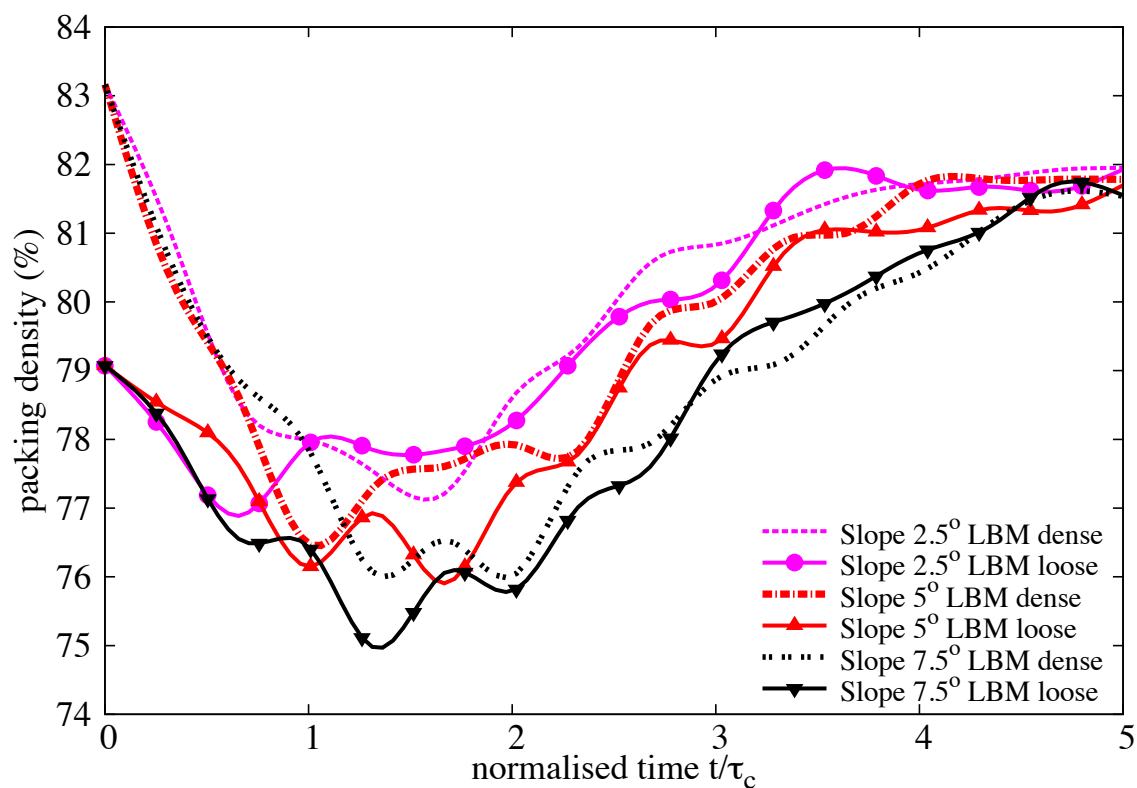


Figure 6.42 Evolution of packing density with time

6 6.3.2 Effect of permeability

7 In DEM, the grain – grain interaction is described based on the overlap between the grains at the
8 contact surface. In a 3D granular assembly, the pore spaces between grains are interconnected.
9 Whereas in a 2-D assembly, the grains are in contact with each other that result in a non-
10 interconnected pore-fluid space. This causes a no flow condition in a 2-D case. In order to
11 overcome this difficulty, a reduction in radius is assumed only during the LBM computation
12 phase (fluid and fluid – solid interaction). The reduction in radius allows interconnected pore
13 space through which the surrounding fluid can flow. This technique has no effect on the grain –
14 grain interactions computed using DEM. See [Kumar et al. \(2012\)](#) for more details about the
15 relationship between reduction in radius and permeability of the granular assembly.

16 For a slope angle of 5°, the hydrodynamic radius of the loosely packed grains was varied
17 from $r = 0.7R$ (high permeability), 0.75R, 0.8R, 0.85R to 0.9R (low permeability). The run-
18 out distance is found to increase with decrease in the permeability of the granular assembly
19 (see [Figure 6.43](#)). The run-out distance for high permeable conditions ($r = 0.7R – 0.8R$) were
20 lower than their dry counterparts. Although, decrease in permeability resulted in an increase
21 in the run-out distance, no significant change in the run-out behaviour was observed for a
22 hydrodynamic radius of up to 0.8R.

23 With further decrease in permeability ($r = 0.85R$ and 0.9R), the run-out distance in the fluid
24 was greater than the run-out observed in the dry condition. At very low permeability ($r = 0.9R$),
25 granular material started to entrain more water at the base, which causes a reduction in the
26 effective stress accompanied by a lubrication effect on the flowing granular media. This can be
27 seen as a significant increase in the peak kinetic energy and the duration of the peak energy, in
28 comparison with dry and high permeable conditions (see [Figure 6.45](#)).

29 The permeability of the granular column did not have an influence on the evolution of
30 height during the flow. However, dry granular column tends to collapse more than the immersed
31 granular column (see [Figure 6.44](#)).

32 Positive pore-pressure generation at the base of the flow was observed for low permeable
conditions. Inspection of the local packing density showed entrainment of water at the base
of the flow, which can also be observed by the steep decrease in the packing density (see [Figure 6.46](#)) for the very low permeability condition ($r = 0.9R$). At the end of the flow ($t \geq 3 \times \tau_c$),
the excess pore-pressure dissipates and the granular material, irrespective of their permeability,
reaches almost the same packing density.

1
2
3
4
5

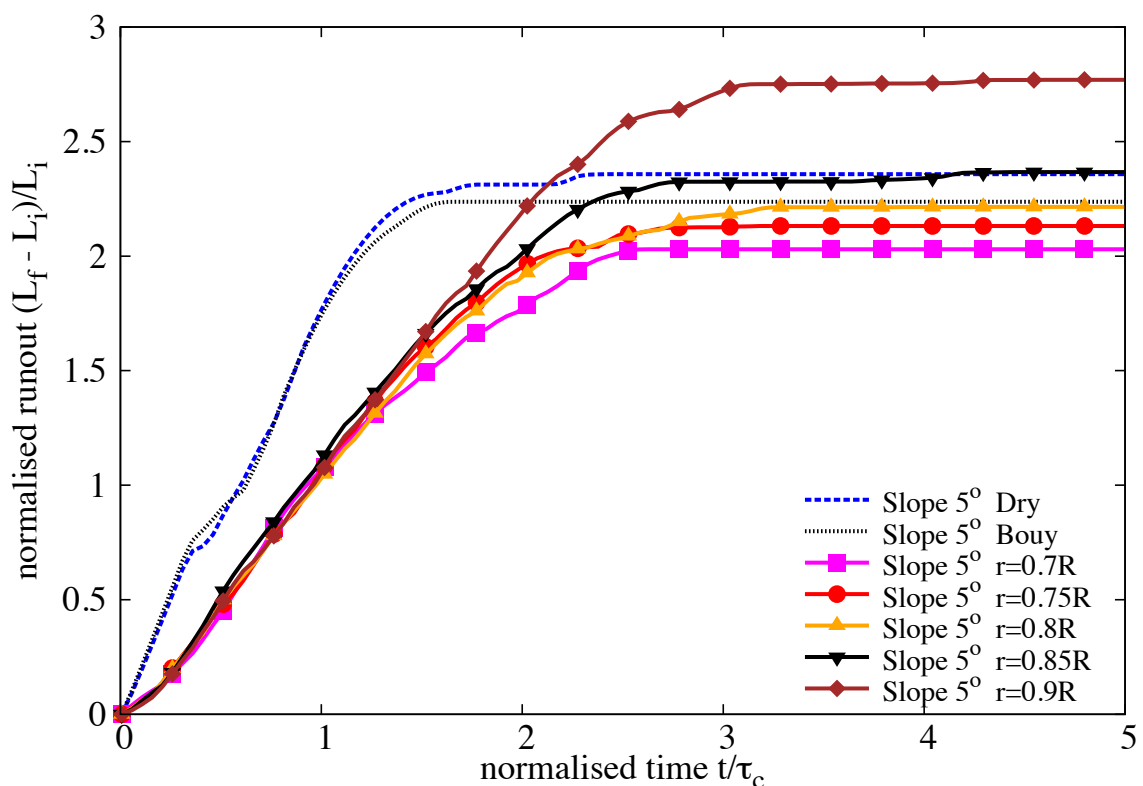


Figure 6.43 Evolution of run-out with time for different permeability (loose slope 5°)

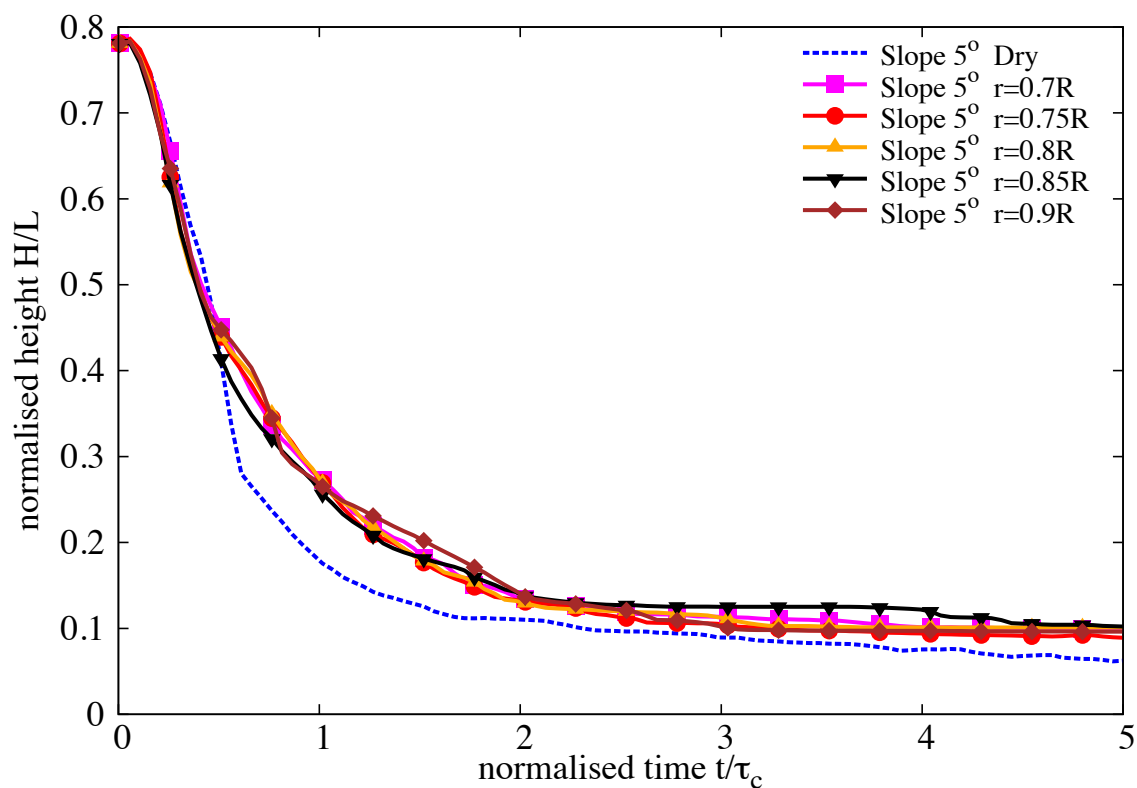


Figure 6.44 Evolution of height with time for different permeability (loose slope 5°)

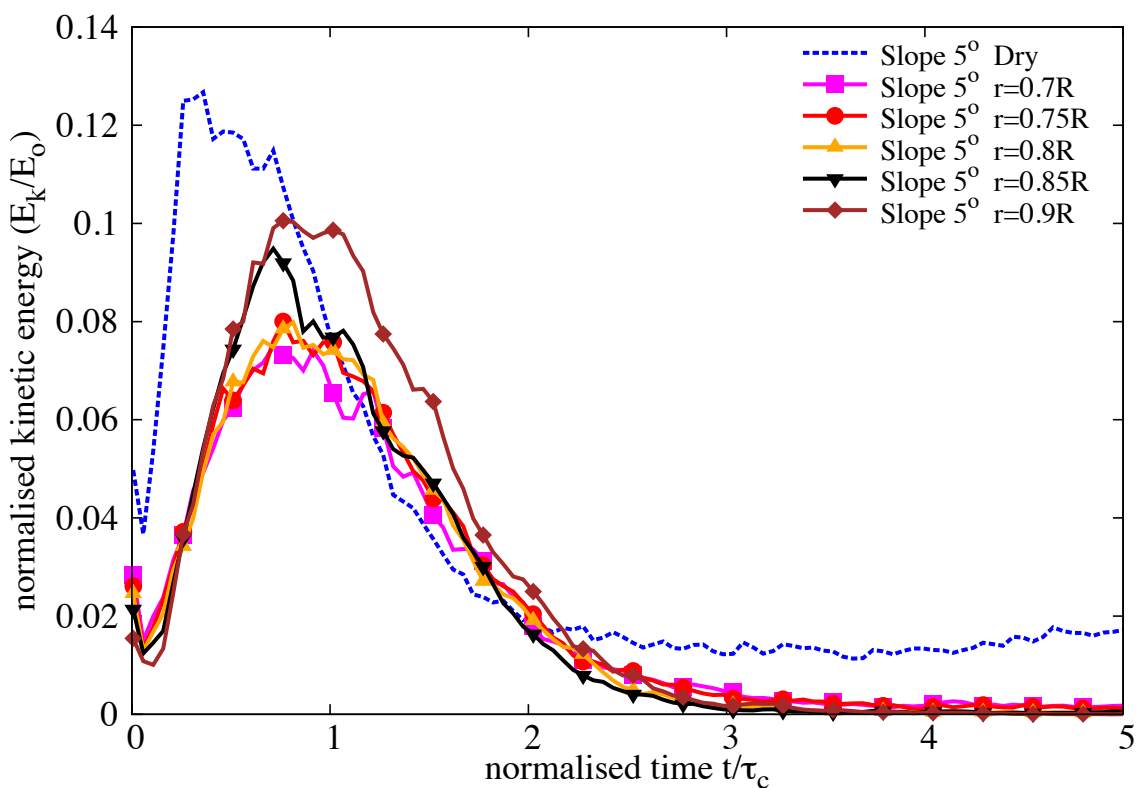


Figure 6.45 Evolution of Kinetic Energy with time for different permeability (loose slope 5°)

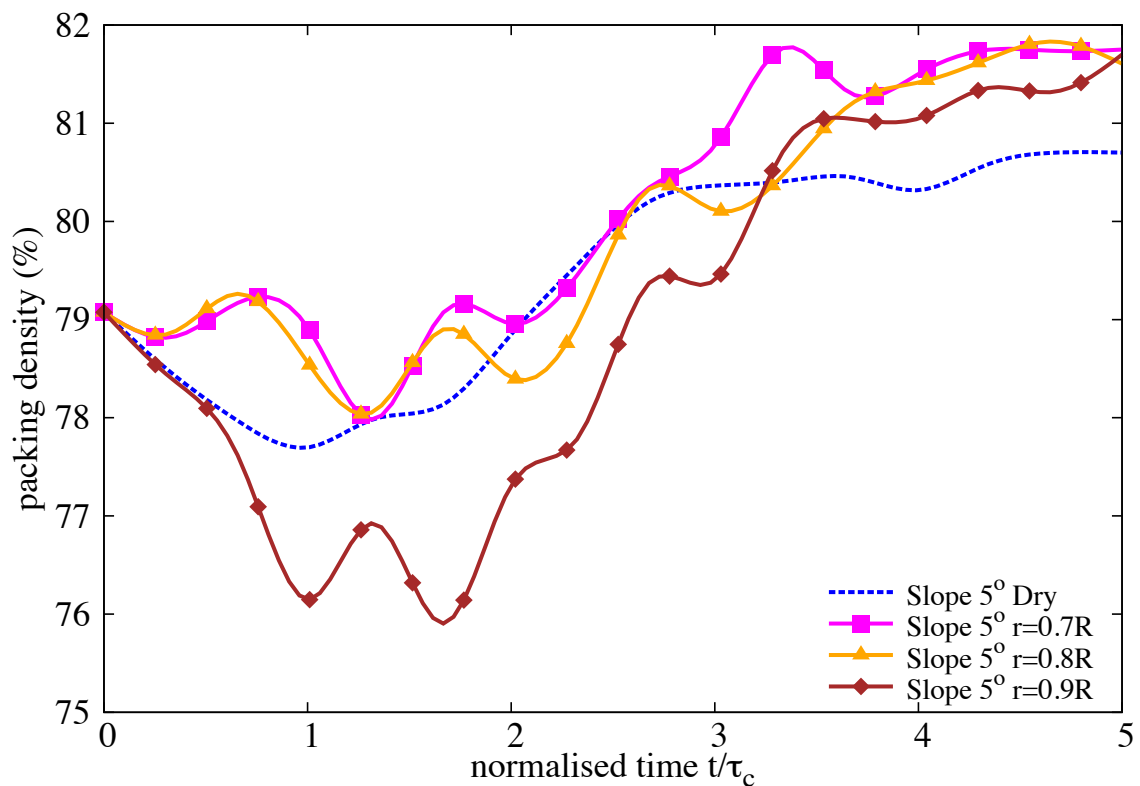


Figure 6.46 Evolution of packing density with time for different permeability (loose slope 5°)

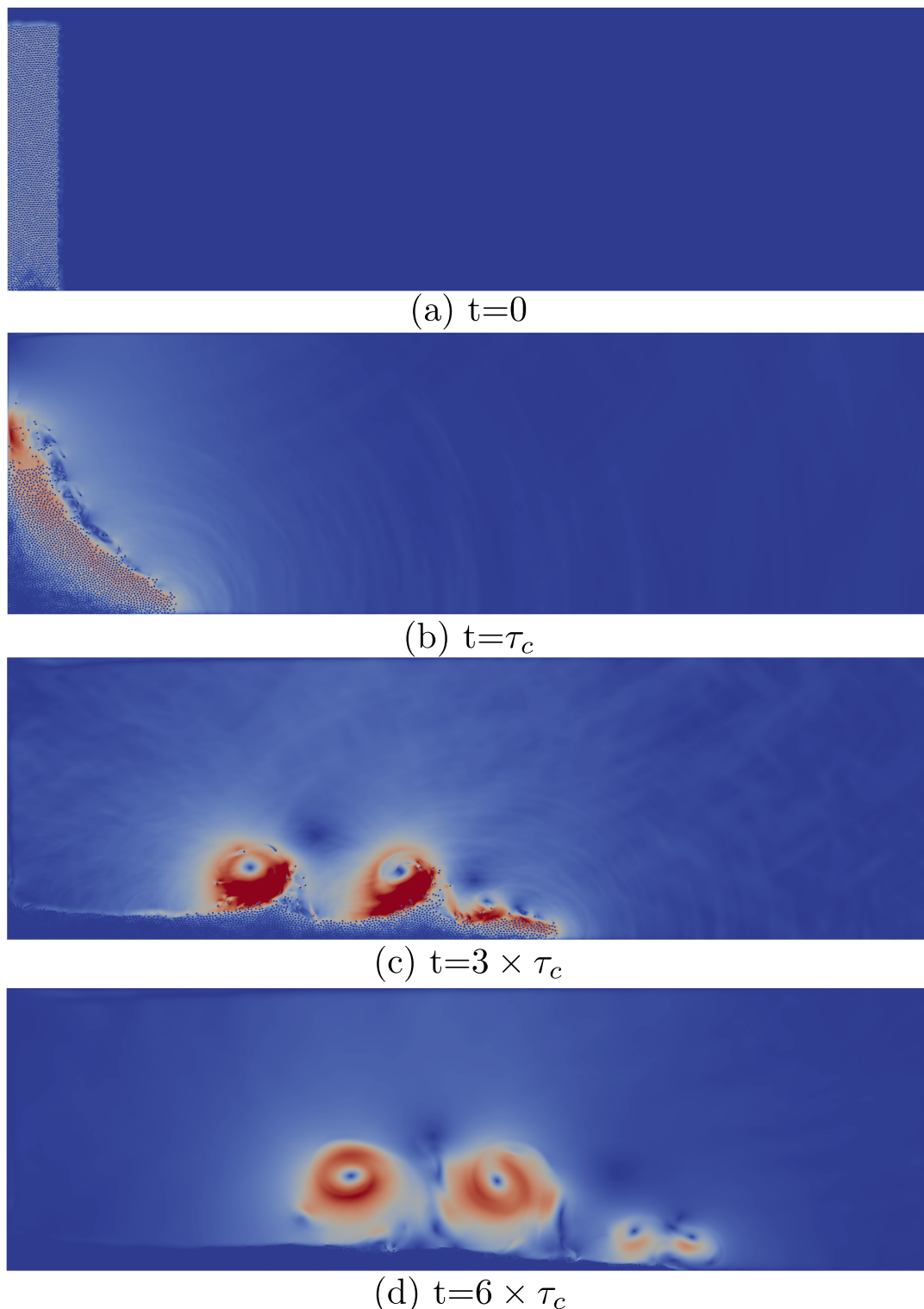
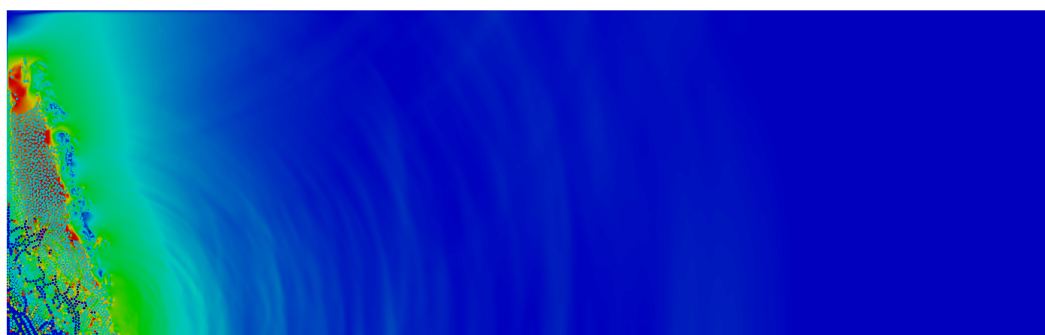
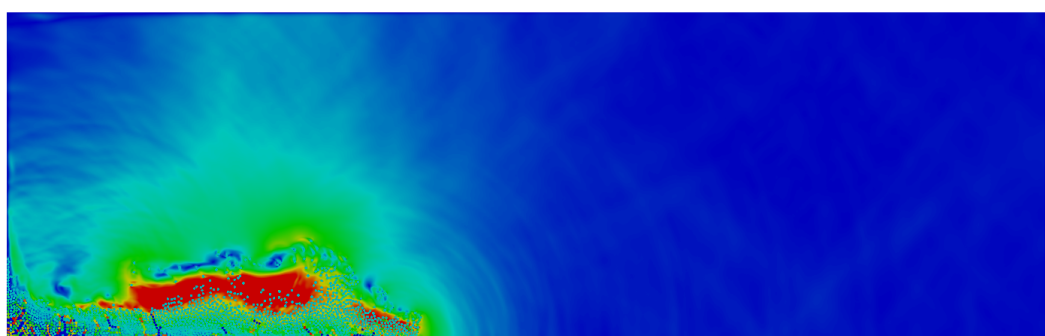


Figure 6.47 Flow evolution of a granular column collapse in fluid ($a = 6$) on a horizontal surface

 $t = 0\tau_c$  $t = 1\tau_c$  $t = 3\tau_c$

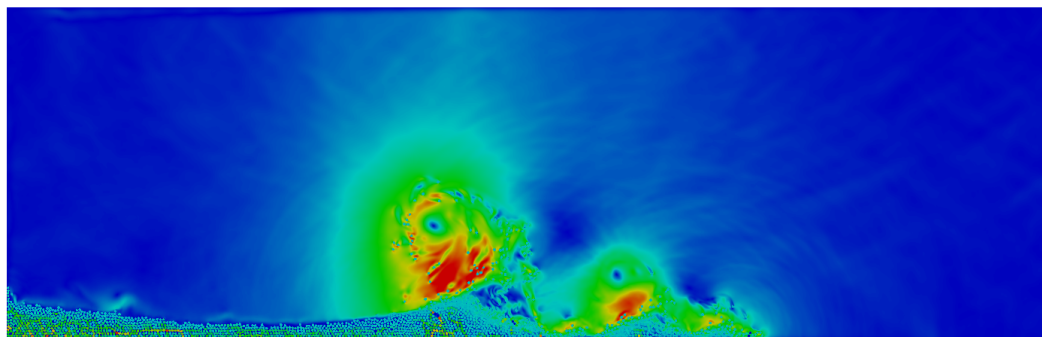
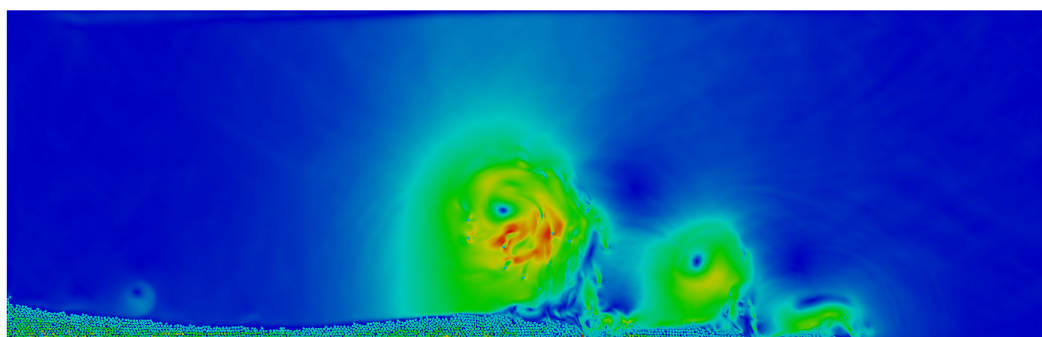
 $t = 6\tau_c$  $t = 8\tau_c$

Figure 6.48 Flow evolution of a granular column collapse in fluid ($a = 6$) on a slope of 5° . Shows the velocity profile of fluid due to interaction with the grains (red - higher velocity).

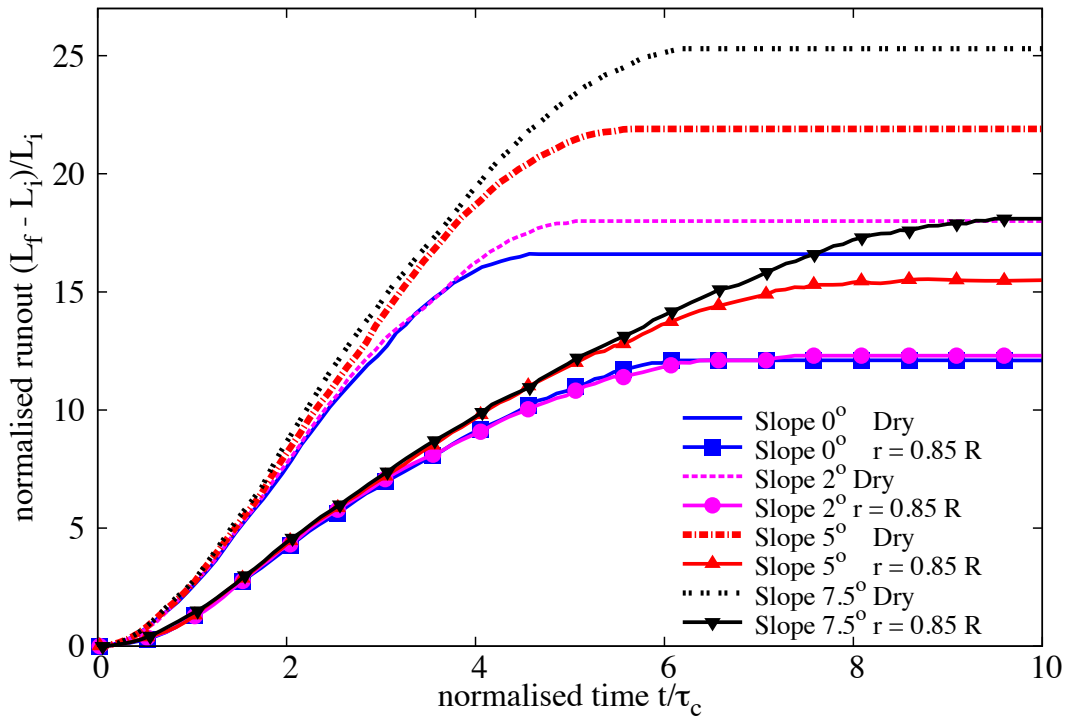


Figure 6.49 Evolution of run-out for a column collapse in fluid ($a = 6$) on a slope of 5°

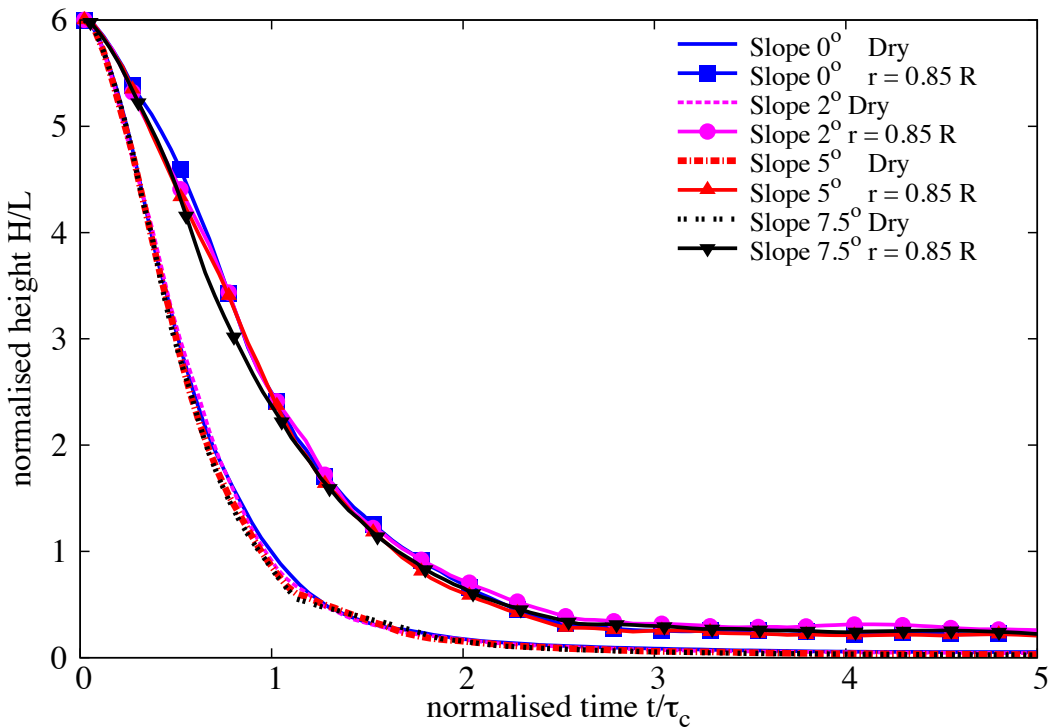
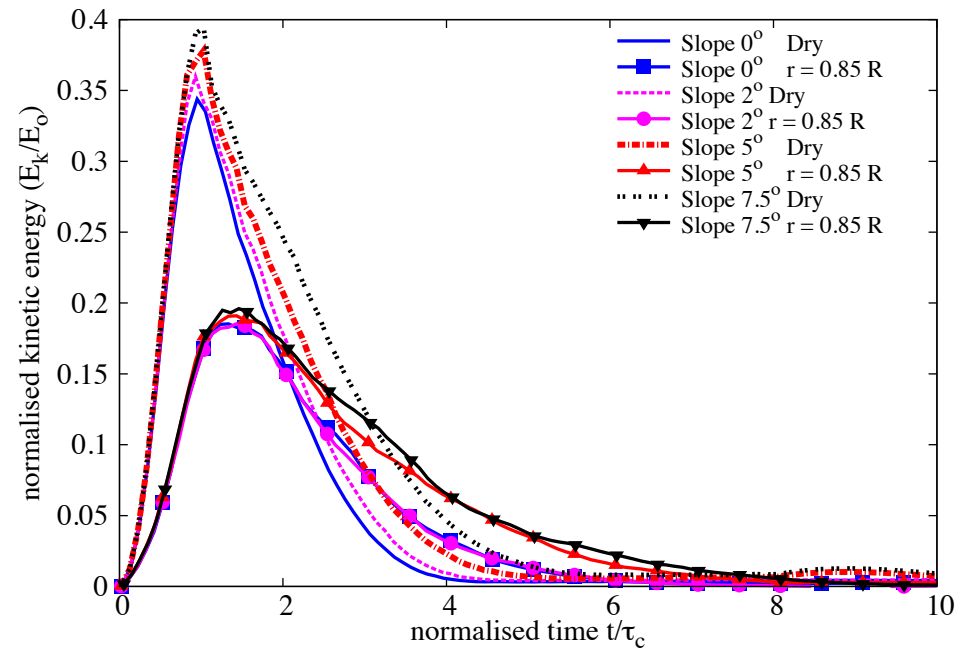
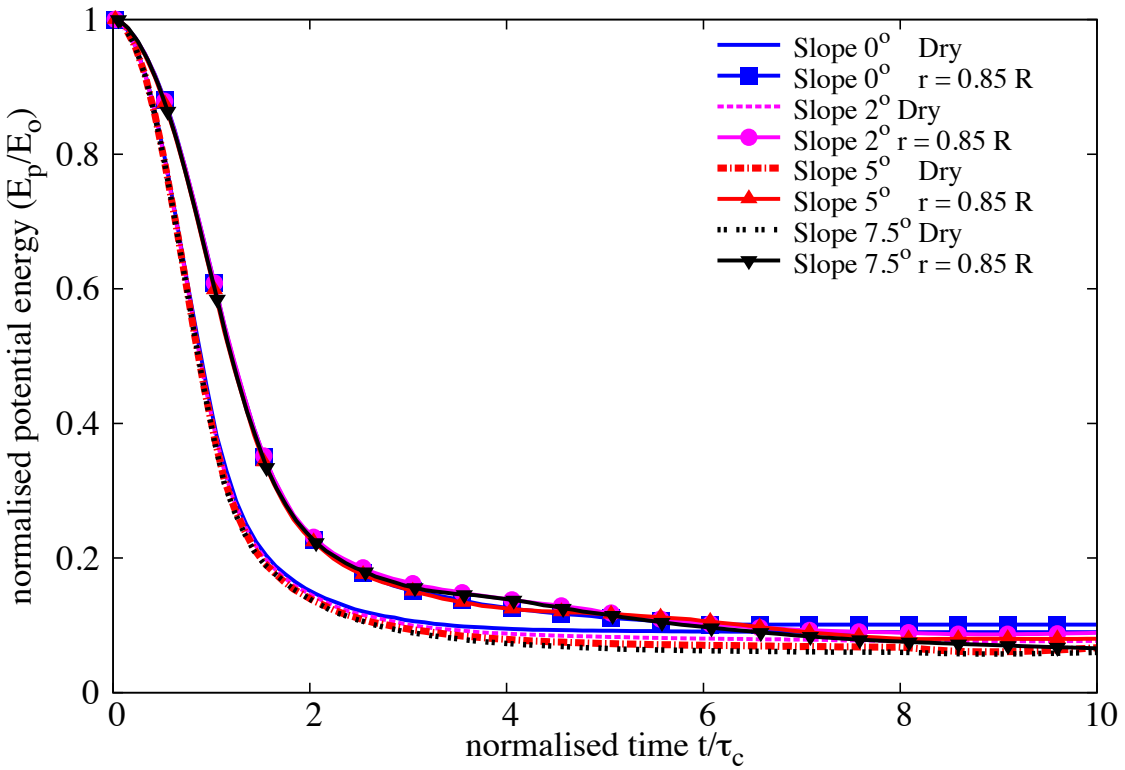


Figure 6.50 Evolution of height with time for a column collapse in fluid ($a = 6$) on a slope of 5°

6.3 Submarine granular flows down incline plane

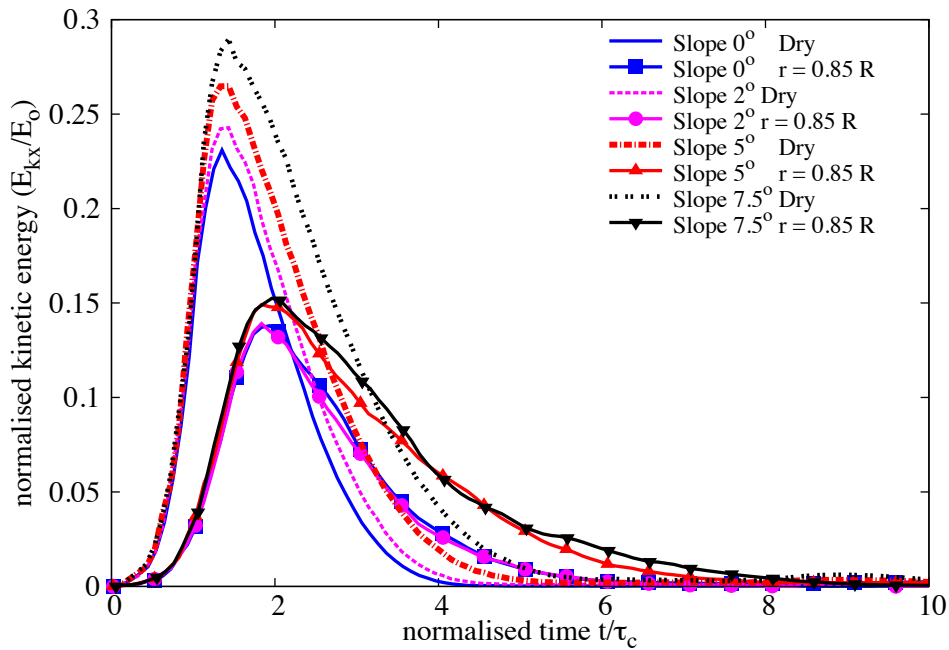


(a) Evolution of the total kinetic energy

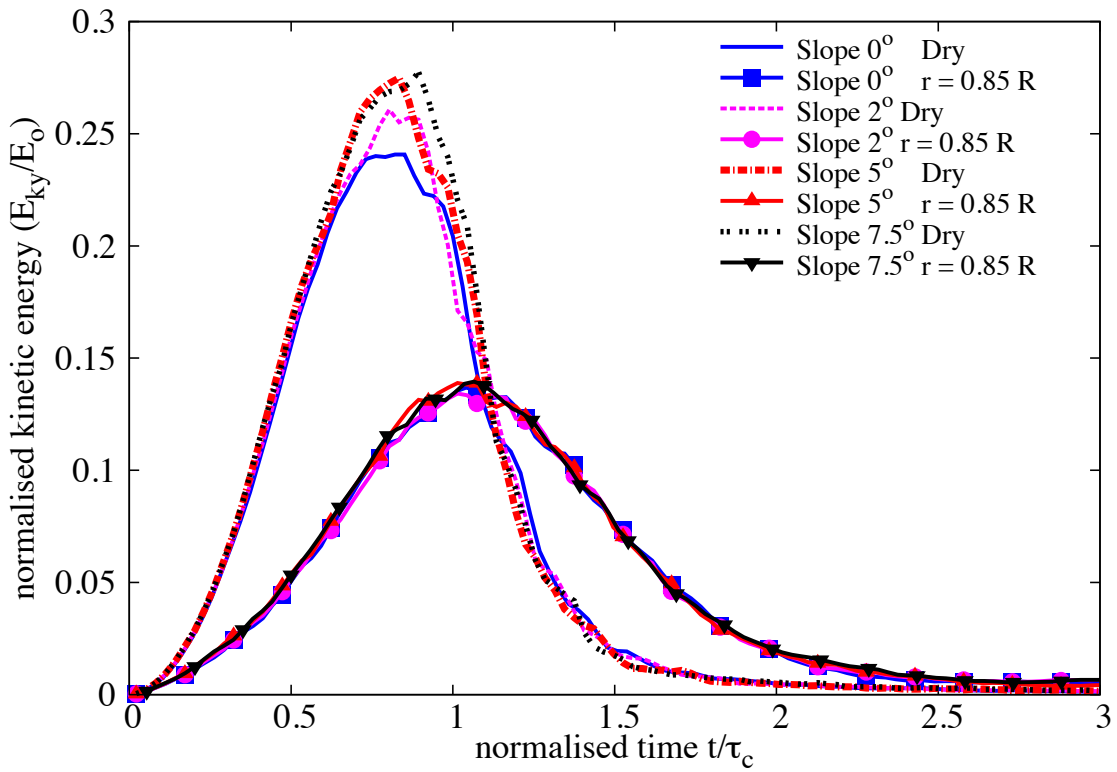


(b) Evolution of the total potential energy

Figure 6.51 Evolution of the kinetic and the potential energy with time for a granular column collapse in fluid (a = 6) on a slope of 5°



(a) Evolution of the vertical kinetic energy



(b) Evolution of the horizontal kinetic energy

Figure 6.52 Evolution of the kinetic energies with time for a granular column collapse in fluid ($a = 6$) on a slope of 5°

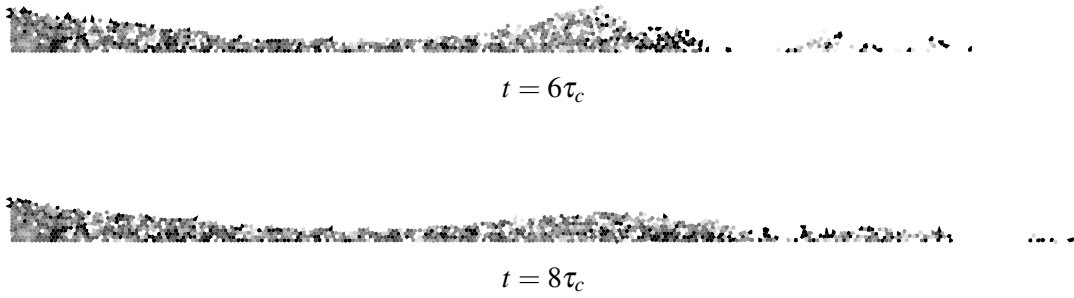


Figure 6.53 Packing density of a granular column collapse in fluid ($a = 6$) on a slope of 5° .

6.3.3 Tall columns

6.3.4 Summary

Two-dimensional LB-DEM simulations were performed to understand the behaviour of submarine granular flows. Unlike dry granular collapse, the run-out behaviour in fluid is dictated by the initial volume fraction. Granular columns with loose packing tend to flow longer in comparison to dense columns, due to entrainment of water at the base resulting in lubrication. The loose column when it starts flowing expands and ejects liquid, leading to a partial fluidization of the material. However, with increase in the slope angle, the run-out in fluid is influenced by the viscous drag on the granular materials. The run-out distance in fluid increases with decrease in permeability. More research work is required to characterise the flow behaviour of granular materials, especially in submerged conditions.

References

6

- Bonnet, F., Richard, T., and Philippe, P. (2010). Sensitivity to solid volume fraction of gravitational instability in a granular medium. *Granular Matter*. 7
8
- Denlinger, R. and Iverson, R. (2001). Flow of variably fluidized granular masses across three-dimensional terrain, ii: Numerical predictions and experimental tests. *J. Geophys. Res.*, 106(B1):553–566. 9
10
11
- Iverson, R. M. (2000). Acute Sensitivity of Landslide Rates to Initial Soil Porosity. *Science*, 290(5491):513–516. 12
13
- Kumar, K., Soga, K., and Delenne, J.-Y. (2012). *Discrete Element Modelling of Particulate Media*. Special Publication. Royal Society of Chemistry, Cambridge. 14
15
- Mansouri, M., Delenne, J. Y., El Youssoufi, M. S., and Seridi, A. (2009). A 3D DEM-LBM approach for the assessment of the quick condition for sands. *Comptes Rendus Mécanique*, 337(9-10):675–681. 16
17
18
- Meruane, C., Tamburrino, A., and Roche, O. (2010). On the role of the ambient fluid on gravitational granular flow dynamics. *Journal of Fluid Mechanics*, 648:381–404. 19
20
- Midi, G. D. R. (2004). On dense granular flows. *European Physical Journal E*, 14(4):341–365. 21
- Pailha, M., Pouliquen, O., and Nicolas, M. (2008). Initiation of Submarine Granular Avalanches: Role of the Initial Volume Fraction. *AIP Conference Proceedings*, 1027(1):935–937. 22
23
- Peker, S. and Helvacı, S. (2007). *Solid-liquid two phase flow*. Elsevier. 24
- Rondon, L., Pouliquen, O., and Aussillous, P. (2011). Granular collapse in a fluid: Role of the initial volume fraction. *Physics of Fluids*, 23(7):073301–073301–7. 25
26
- Thompson, E. L. and Hupper, H. E. (2007). Granular column collapses: Further experimental results. *Journal of Fluid Mechanics*, 575:177–186. 27
28
- Topin, V., Dubois, F., Monerie, Y., Perales, F., and Wachs, A. (2011). Micro-rheology of dense particulate flows: Application to immersed avalanches. *Journal of Non-Newtonian Fluid Mechanics*, 166(1-2):63–72. 29
30
369
- Topin, V., Monerie, Y., Perales, F., and Radjaï, F. (2012). Collapse Dynamics and Runout of Dense Granular Materials in a Fluid. *Physical Review Letters*, 109(18):188001. 370
371
- Yazdchi, K., Srivastava, S., and Luding, S. (2011). Microstructural effects on the permeability of periodic fibrous porous media. *International Journal of Multiphase Flow*. 372
373